UNIVERSITÀ DEGLI STUDI DI PADOVA
SCUOLA DI INGEGNERIA

CORSO DI LAUREA MAGISTRALE IN INGEGNERIA CIVILE
Dipartimento di Ingegneria Civile, Edile ed Ambientale - DICEA

Tesi di laurea magistrale

NONLINEAR ANALYSIS OF REINFORCED CONCRETE BUILDINGS UNDER SEISMIC LOADS

Relatore: Prof. Ing. Secchi Stefano
Correlatori: Prof. Raguenenau Frédéric
Prof. Giry Cedric

Laureanda: Bittante Giulia
Matricola: 1041333

Anno Accademico 2014 - 2015

ABSTRACT

Earthquakes are natural phenomena occurring very often all around the world and bringing destruction and death. Over the past years, with the help of computers and computational methods, several seismic analyses procedures have been developed but, because of their diversity, the results could be meaningfully scattered so that various campaigns have been launched to uniform and validate them.

In particular SMART 2013 benchmark consists in testing on a shaking table a reinforced concrete scaled structure and compare the results coming out from the numerical models to those experimentally measured.

In this paper, after the description of the mock-up, the numerical model is given: 3D elements are chosen for modelling concrete parts while beams are chosen for steel reinforcement bars. The choice of a continuum-damage-based constitutive law for concrete lets obtain a concrete behavior performance close to the real one, including micro cracking, internal sliding and other local phenomena, and lets easily identify damage localization. For the steel an uniaxial law is computed, without making the computational cost augmenting.

The seismic inputs are given under the form of imposed displacements at the structure bases and they correspond to real earthquake accelerograms, from 0.2g to 1.70g.

The numerical results are then displayed and compared to the experimental ones and at the end, they're even compared to those coming out from an elastic constitutive law model, in order to obtain a strength reduction factor commonly used in simplified seismic analyses.

TABLE OF CONTENTS

1 INTRODUCTION

Every year more then 400 000 earthquakes can be detected with current instrumentation and luckily only 1/5 of them can be felt. But when a strong seismic event occurs, it often causes destruction and death, as Haiti 2010 (316000 people killed, 1,3 million displaced, 97000 houses destroyed), Sumatra 2004 (220000 killed, 17 million displaced) and many others (USGS).

Nowadays seismic rules for buildings design have been introduced and different kind of seismic analysis have been developed in order to predict structural behavior of buildings and prevent damage, collapse and, the most important, save human lives.

Because of their quasi-brittle behavior, reinforced concrete buildings require a special attention: very little is known about nonlinear range and torsional 3D effects. The aim of the several campaigns launched in the past decades was to investigate over non linearity and try to validate different ways of structure modeling and analyzing but, as the SMART 2008 (Seismic design and best-estimate Methods Assessment for Reinforced concrete buildings subjected to Torsion and non-linear effects) campaign underlined, the results are nowadays very scattered.

1.1 SMART 2008

In 2007, the CEA (Commissariat à l'Énergie Atomique et aux énergies alternatives) and EDF (Électricité de France) launched a blind prediction contest, involving 35 institutions from 20 countries all over the world in order to assess capability of RC structures exhibiting 3D effects to withstand earthquake load.

The main objectives of this benchmark were to:

- assess different conventional design methods of structural dynamic analyses, including floor response spectra evaluation;
- compare best-estimate methods for structural dynamics response and floor response spectra evaluation.

In order to achieve these objectives, an asymmetric 3-storeys RC mock-up was defined, representing a half of a nuclear building, and all the geometry and material prescriptions were given to the participants. This specimen was then built and tested on a shaking table (Azalee) following a list of seismic loads (21 runs) and displacements and damage data were recorded.

Every participant was supposed to create his own numerical model of the mock-up, opting for the program and the finite element type he preferred and send back the outputs (displacements) obtained by the chosen analysis type.

The organizing committee was then charged to compare the experimental data with the ones provided by all the participants and a final report was written.

The conclusions of this blind predicting benchmark were (Lermitte, 2008):

1. there's a huge variability in participants hypothesis (type of model, material properties, damping values, mass modeling, type of analysis...), which leads to very scattered results and it underlines the necessity to reconsider something in engineers practice;
2. some guidelines should be given to participants in order to:
    - simplify the type of the model for conventional analyses;
    - use the damping value according to the type of analysis (because of the high influence of damping in the structure behavior, research should be undergone);
    - choose a right Young modulus and his law of degradation due to damage;
3. more complete studies investigating the parameters variability influence in conventional analyses should be started.

In 2011 was then launched a new experimental campaign, SMART 2013, with the same objectives as the 2008 one, taking account the previous suggestions and conclusions.

1.2 THESIS OVERVIEW

This paper purpose is to illustrate the choices and procedures made at LMT Cachan, taking part at the SMART 2013 project.

Firstly the SMART 2013 campaign will be illustrated, focusing on requests and objectives of the benchmark and the main modelling choices are outlined.

In the following chapter it will be presented the geometrical model and the detailed Finite Elements Model computation, the material laws for steel and concrete will then be investigated and a description of the applied time-history algorithm is exposed.

After reporting a small chapter about computational problems, the results are conferred and conclusions are written.

2 THEORETICAL BACKGROUND

2.1 SMART 2013

As for the project SMART 2008, the benchmark 2013 aim is to raise knowledge of RC buildings behavior due to seismic loadings with particular attention to non-linear and torsional 3D effects.

The objectives are exactly the same as for the previous campaign:

- comparison and validation of approaches used for the dynamics responses;
- assessment of the capability of advanced dynamic non-linear models for predicting structures behavior;
- quantification of the vulnerability within a probabilistic framework.

The main differences between the two benchmarks are that in the current one:

- Advanced digital image correlation techniques are used to monitor the displacements in some established points and the boundary conditions;
- natural signals are used as input ground motions;
- a new strong reinforced concrete foundation has been designed;
- an accurate finite element model of the shaking table is provided by CEA;
- higher seismic inputs are prescribed;
- material parameters and damping values guidelines are given.

This international benchmark is composed by four stages. The stage#1 requires a general description of the numerical model , including information about the name and type of the fem code used, descriptions of the time integration algorithm, damping value, finite

elements and degrees of freedom, constitutive laws taken in account for concrete and steel (local tests are prescribed)... During the stage#2 the elastic calibration is performed: after considering the results of the modal analysis, light seismic loads are applied in order to characterize the linear behavior of the numerical model. The following stage concerns the blind nonlinear computation: higher seismic inputs are applied in order to enter the nonlinear range of constitutive laws and the consequent displacement field will be sent to the organizing committee and then compared to the experimental results. The last part of the benchmark consists in conducting vulnerability analyses for determining fragility curves (stage#4) (Chaudat & Richard, 2013).

2.1.1 SEISMIC ANALYSES

During the past years, owing to the progress of the fem method and to the growing efficacy of computers, several seismic analyses methods have been developed and implemented.

First of all a *modal analysis* has to be conducted in the interest of identifying the shaking characteristics of the structure. It consists in solving the eigenvalue problem:

$$[M]\left[\ddot{U}\right] + [K][U] = [0]$$

standing out from the classical equation of motion of a spring mass system, where the damping is consider equal to zero. The eigenvectors are representative of the natural mode shapes, corresponding to the natural frequencies (eigenvalues) of the structure.

The most simplified analysis is the *equivalent static* one, which consists in translating the earthquake ground accelerations into static forces applied to the building, which is supposed to respond according to his fundamental modes. This case could be applied when the structure shows high regularity and symmetry (low importance of torsion) and corrected with some factors to account effects of yielding or small irregularities.

One step closer to real behavior of buildings is given by the *response spectrum analysis*, in which, for each solicitation the corresponding natural frequency is read in the design spectrum and then they are combined in three possible ways: absolute (peak values are added together), square root of the sum of the squares (SRSS), complete quadratic combination (CQC).

As the seismic inputs become stronger and the nonlinear domain is reached, it's possible to choose a *pushover analysis* (nonlinear static). The structure is still represented by a SDOF system, but with nonlinear properties and the ground accelerations are plotted as

total force against a reference displacement in a capacity curve, then combined with the response spectrum.

When higher natural modes become important, the static analyses are no longer appropriate. In case of remaining in the linear field of materials behavior the *linear dynamic analysis* can be applied: the structure is modeled as a MDOF system and the inputs (seismic solicitations) and outputs (stresses and displacements) are calculated in the time domain. All phase information is maintained and higher natural modes can be taken in account (taller buildings).

Once again the demand of going up to the nonlinear part of material laws requires a more complex analysis: the *nonlinear dynamic*. With it both the constitutive law and the loadings are integrated in the time domain and the result is a response curve for each degree of freedom considered. This last kind of analysis can be applied to irregular buildings and its results are very accurate, however the response is very sensible to parameters variations and the calculations are heavy.

2.1.2 FEM METHOD AND MODELLING CHOICES

The FEMethod is an approximate way to solve the mechanics problem: the continuum body is discretized into representative geometrical elements and for each one of their nodal points, the state variables are computed.

Depending on the shape of the considered body and on the accuracy needed, one can choose between three main formulation families:

- Beam/truss when one dimension is greater than the other two. The beam elements has only two nodes at the ends and for each node 3 degrees of freedom are considered (DOF), while the truss accounts only one.
- Plate/shell when two dimension are considered. The difference between shell and plate lies in the out-of-plane formulation.
- Bricks when a 3D problem is considered.

More specifically a continuum body can be represented as fig.1 shows

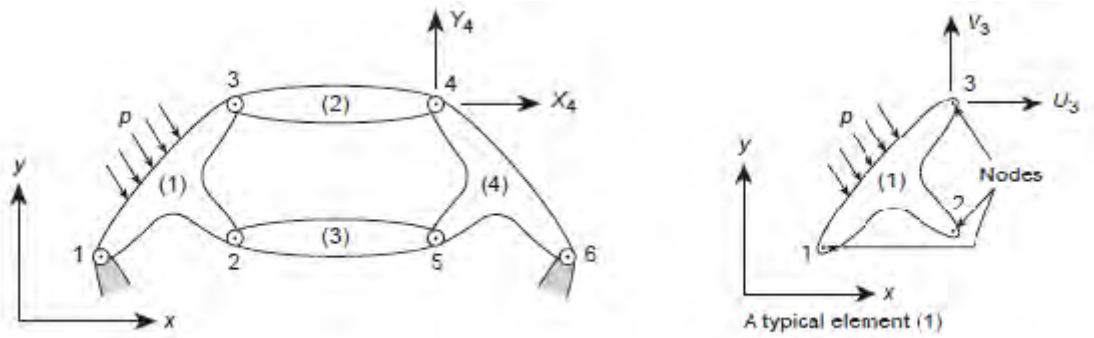

Figure 1: Continuum body discretization

Where forces and displacements could be listed as nodal-equivalent ones:

$$q = \begin{Bmatrix} q_1 \\ q_2 \\ \dots \end{Bmatrix} \text{ with } q_i = \begin{Bmatrix} U_i \\ V_i \end{Bmatrix} \text{ nodal forces}$$

$$a = \begin{Bmatrix} a_1 \\ a_2 \\ \dots \end{Bmatrix} \text{ with } a_i = \begin{Bmatrix} u_i \\ v_i \end{Bmatrix} \text{ nodal displacements}$$

For an elastic problem: $q^1 = K^1 a_1 + f_p^1 + f_{\varepsilon 0}^1$ which represents the equilibrium between internal and external forces.

For the equivalence with the stresses matrix it could be written:

$$\sigma^1 = Q^1 a_1 + \sigma_{\varepsilon 0}^1 \text{ where Q is the element stresses matrix}$$

Introducing the boundary conditions:

$$K^i a_i = r - f$$

a standard discrete system could be written as

$$Ka + f = r, \text{ with } K = \sum K^e.$$

Considering a single finite element e, with nodes i, j, m etc. any characteristic field in any point of the element can be written in terms of nodal formulation:

$$u = \bar{u} = \sum N_k a_k^e = Na^e \text{ with } Ni = NI \text{ for displacements}$$

$$\varepsilon = \bar{\varepsilon} = Su = Ba \text{ with } B = SN \text{for strains}$$

$$\sigma = D(\varepsilon - \varepsilon_0) + \sigma_0 \text{ for stresses, where D is the constitutive matrix.}$$

In order to make the nodal forces equal to the boundary stresses and the external forces a virtual displacement δa^e is considered:

$$\delta u = N\delta a^e \text{ and } \delta\varepsilon = B\delta a^e$$

leading to:

$$q^e = \int_V B^T \sigma dV - \int_V N^T b dV.$$

Knowing that

$$q^e = K^e a_e + f^e,\ K^e = \int_V B^T D B dV \text{ (being B=SN)}$$

$$\text{and } f^e = -\int_V N^T b dV - \int_V B^T D\varepsilon dV + \int_V B^T \sigma_0 dV.$$

For the whole structure is $u = \bar{N}a$, with a being the list of points.

For any virtual displacement, being

$$-\delta a^T r = \int_V \delta u^T b dV + \int_A \delta u^T t dA - \int_V \delta \varepsilon^T \sigma dV$$

$$Ka = r - f$$

$$f = -\int_V N^T b dV - \int_A N^T t dA - \int_V B^T D\varepsilon_0 dV + \int_V B^T \sigma_0 dV,$$

ensuring the satisfaction of the equilibrium equations.

When considering complicated systems, involving a lot of points, it becomes more difficult to ensure the equilibrium at all points and another procedure can be introduced: the variational principles. It consists in considering $\delta a, \delta u, \delta \varepsilon$ as variations:

$\delta(a^T r + \int_V u^T b dV + \int_A u^T t dA) = -\delta W$ with W being the potential energy of external loads

$\int_V \delta \varepsilon^T \sigma dV = \delta U$ with U being the strain energy

$$U = \frac{1}{2}\int_V \varepsilon D^T \varepsilon dV - \int_V \varepsilon^T D\varepsilon_0 dV + \int_V \varepsilon^T \sigma_0 dV.$$

The principle lays in the minimization of the total potential Π, which has to be stationary:

$$\delta(U + W) = \delta\Pi = 0.$$

The variational method solution is then depending on the integral approximation procedure chosen, as for example the Ryleigh-Ritz or the Galerking weighted residual. (Zienkiewicz & Taylor)

The FEM softwares are nowadays built for solving a wide range of mechanical problems, and let engineers model and analyze structures in simplified or sophisticated ways, depending on the options chosen (kind of mesh element, linear or polynomial shape functions…).

2.2 LMT CHOICES AND INTERNSHIP OBJECTIVES

The purpose of this paper is to explain the choices made, once decided to participate at the SMART 2013 project, and to validate the described procedure for analyzing RC structures under seismic loads.

The Laboratoire de Mécanique et Technologie de l'Ecole Normale Supérieure de Cachan is a research unit specialized engineering sciences: materials mechanics, experimental mechanics, numerical simulation and high performance computation and it's taking part in the project SMART 2013, presenting his own model.

According to the project requests and to the researchers team knowledge in numerical computation and materials laws, it was possible to tune up a complex numerical model, well representing the real behavior of the structure when cyclic solicitations induced by an earthquake occur.

The brittle behavior of concrete and the high intensity of seismic loadings require the involvement of 3D cubic elements in the numerical model in order to obtain a realistic simulation of torsional effects and a detailed mapping of the damaged zones.

Knowing that such a detailed and complex analysis leads to a very high computational cost, which is not useful to be applied in everyday engineering works, the results will be compared to a simplified elastic model in pursuance of obtaining a Strength Reduction Factor.

The descriptions of geometry, constitutive laws and numerical procedures will be detailed in the following chapters.

3 MATERIALS AND METHODS

3.1 SMART MOCKUP

The SMART 2013 project consists in analyzing a reinforced concrete building, tested on a shaking table (Azalee) in order to obtain the structure response when an earthquake happens. A scaled model representing an half part of an electric building of a nuclear center is built and anchored to the shaking table.

In the following sections will be reported the geometry, materials and fem model in detail.

3.1.1 SUPERSTRUCTURE

The benchmark participants are provided of an accurate description of the structure: it's made by an asymmetric 3 story RC model with trapezoidal base, representing a simplified half part of an electrical nuclear building. The building is scaled to ¼ and the distance between two levels is 1.2 m, reaching a total height of 3.6 m. The three perimetal walls are disposed over a “C”, two of them exhibiting openings, and in the fourth side a column arises, as shown in figures 2,3 and 4.

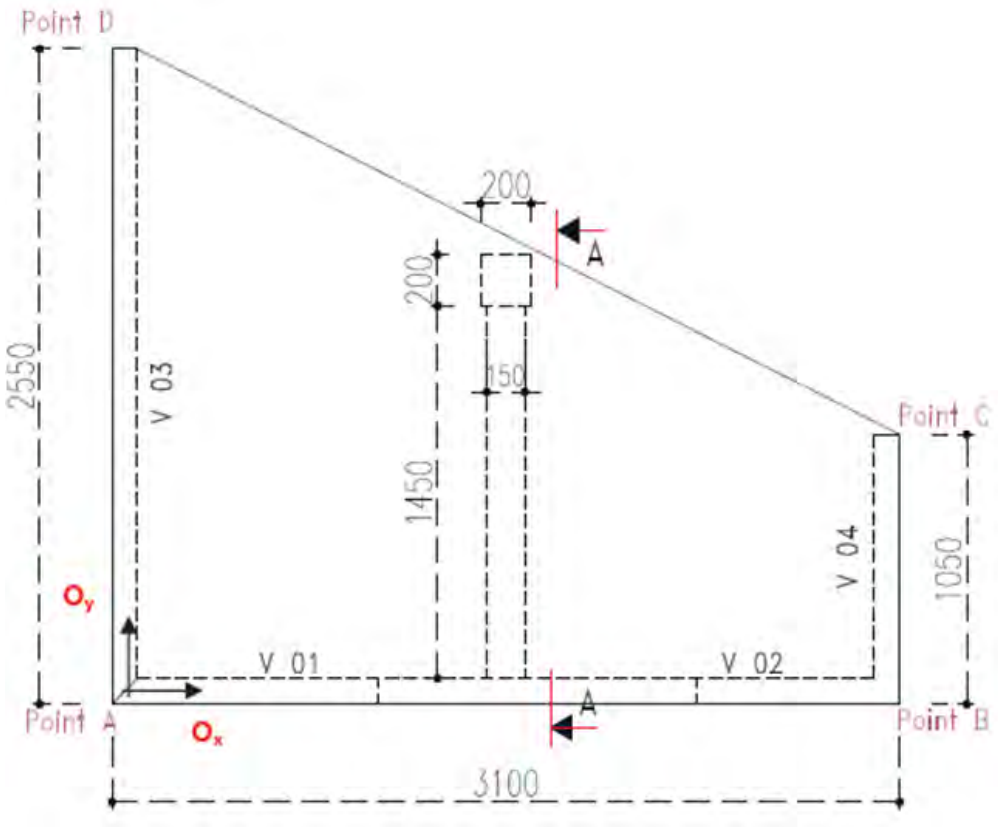

Figure 2: plan of the mock-up

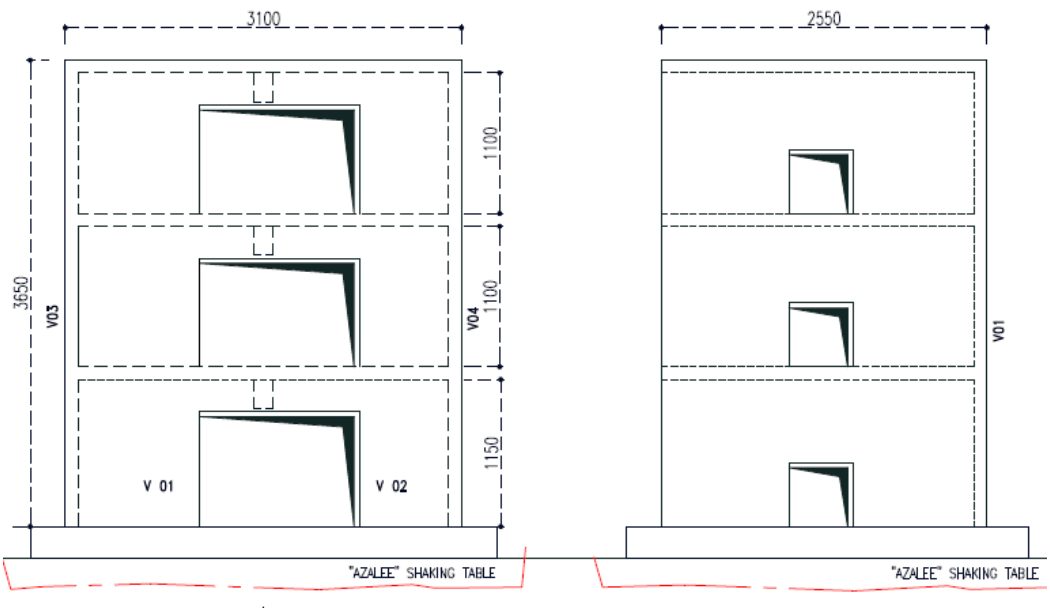

Figure 3: elevation of the mock-up

Figure 4: tested RC scaled building

Reducing the structure dimension to the scale of ¼ leads to the problem of modifying the scale of the length-derived dimensions. In order to conserve acceleration when referring to the scaled model, and knowing that the gravity load and the material properties can't be modified, a scaling factor of 1/16 and ½ are going to be applied to the mass and time respectively.

In the interest of obtaining the scaling factor for all the dimensions, the conservation of accelerations and stresses is imposed:

$$\frac{[length]}{[time]^2} = \frac{[L]}{[T]^2} = constant \rightarrow \lambda = \frac{T^2}{T'^2}$$

$$\frac{[force]}{[length]^2} = \frac{[M][L]}{[T]^2[L]^2} = constant \rightarrow \lambda = \frac{MT'^2}{M'T^2}$$

from which one can achieve:

$$T = \sqrt{\lambda}T' \; and \; M = \lambda^2 M'$$

Being λ=4 the scaling factors become those presented in the table 1.

Table 1: scaling factor

Parameter	Scaling factor
Length	4
Mass	16
Time	2
Acceleration	1
Stress	1
Frequencies	0.5
Forces	16
Steel area	16

In consideration of the previous reflections, the specimen mass had been corrected by anchoring additional masses at each level as shown in the table 2.

Table 2: additional masses

Level	Mean values (tons)
#1	11.45
#2	12.17
#3	10.32

The materials used for building the mockup are concrete C30/37 (for the walls, the central column and the floors) and steel (under the form of reinforcement bars) which properties are experimentally measured and listed in table 3.

Table 3: material parameters

Properties	Concrete	Steel
Young Modulus E [Pa]	$30*10^9$	$200*10^9$
Density ρ [kg/cm^3]	2300	7850
Poisson's coeff. v	0.2	0.3
Compression stress [MPa]	$30*10^6$	$600*10^6$
Traction stress [MPa]	$2.4\ 10^6$	$600*10^6$

With these properties, the superstructure weights 11.89 tons while considering the mass correction 45 tons are reached.

3.1.2 SHAKING TABLE

The dynamic inputs are provided by exciting a shaking table: comparing a shaking table based experiment to a reaction wall based one (fig. 5), the degrees of freedom of the superstructure are not forced to follow imposed displacements and as a result of it, they'll be more realistic.

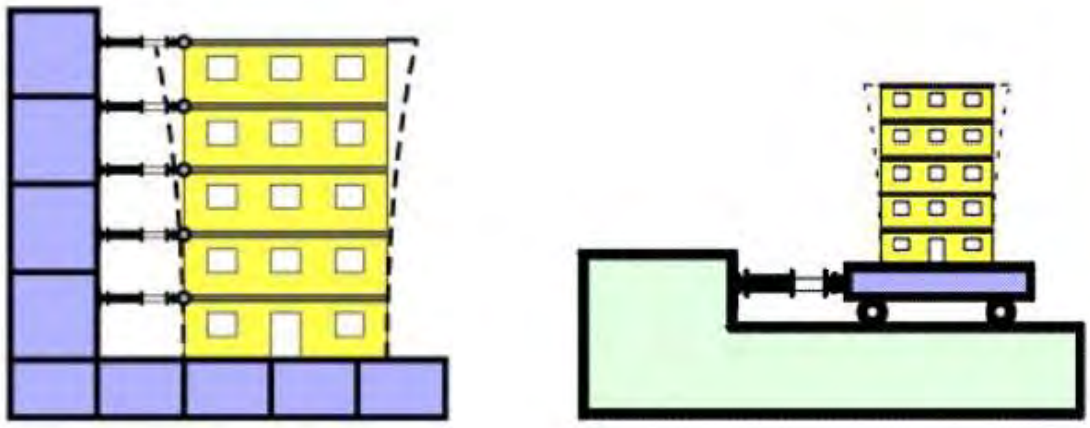

Figure 5: reaction wall and shaking table principles

The shaking table AZALEE is a semi rigid block (6 m x 6 m) which total mass is about 25 tons and it's able to test structures up to 100 tons (fig. 6).

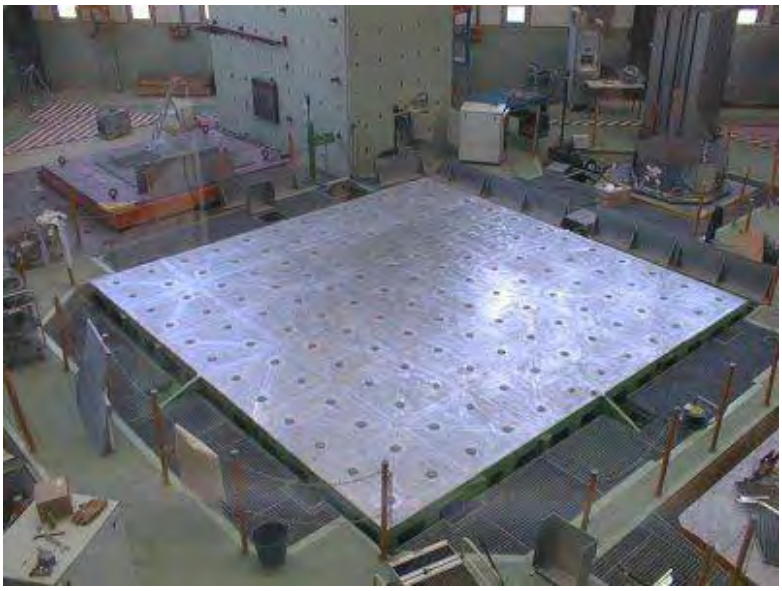

Figure 6: Azalee shaking table at CEA

Eight hydraulics jacks allow to shake the buildings in the three directions: 4 of them are positioned horizontally (2 along x and 2 along y axes) and 4 vertically and as a consequence of that, the superstructure is able to move following all the six degrees of freedom (3 displacements and 3 rotations). The jacks maximal extension is 125 mm along x and y and 100 mm along the vertical axis and each one can transmit the maximal force of 1000 kN.

A system of accumulators positioned under the table and a reaction mass, as the scheme in fig. 7 shows, are necessary to keep the shaking table isolated.

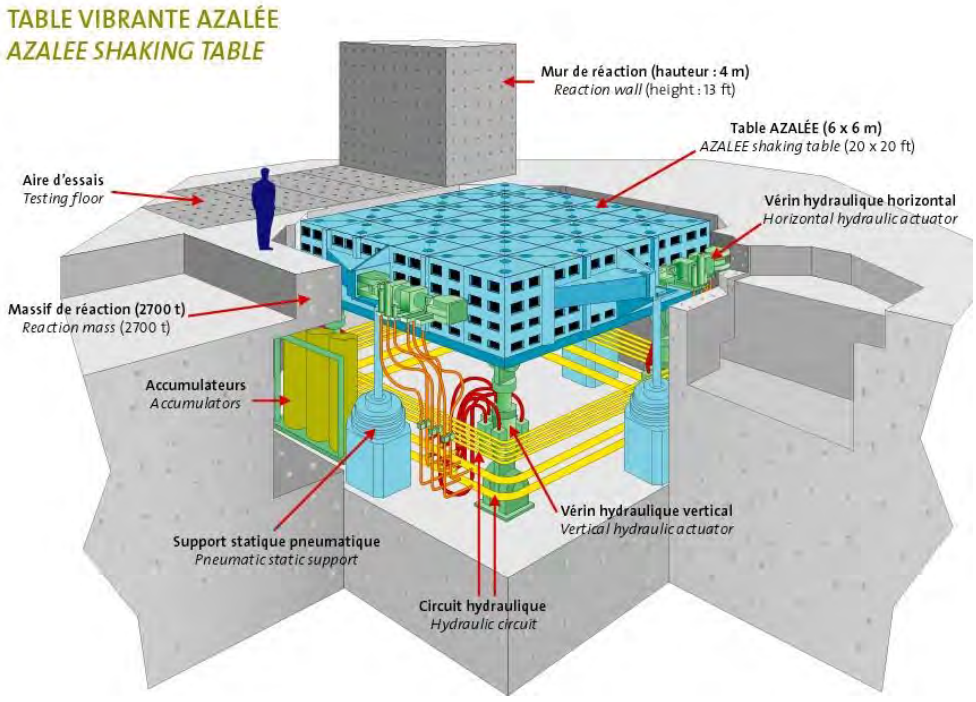

Figure 7: Azalee shaking table scheme

3.1.3 ASSEMBLY

The foundations of the superstructure consist of a continuous footing under the perimetral walls (65 cm wide and 25 cm high) in reinforced concrete and it allows to reduce a the differential settlement between the shaking table and the mockup. The footing is anchored to the shaking table by steel stud bolts, while the central column is fixed to the table by means of a steel plate 2 cm thick.

It's important to underline that the superstructure has been positioned in pursuance of making his center of mass coincide with the one of the shaking table (fig. 8): no additional torsion effect will be induced.

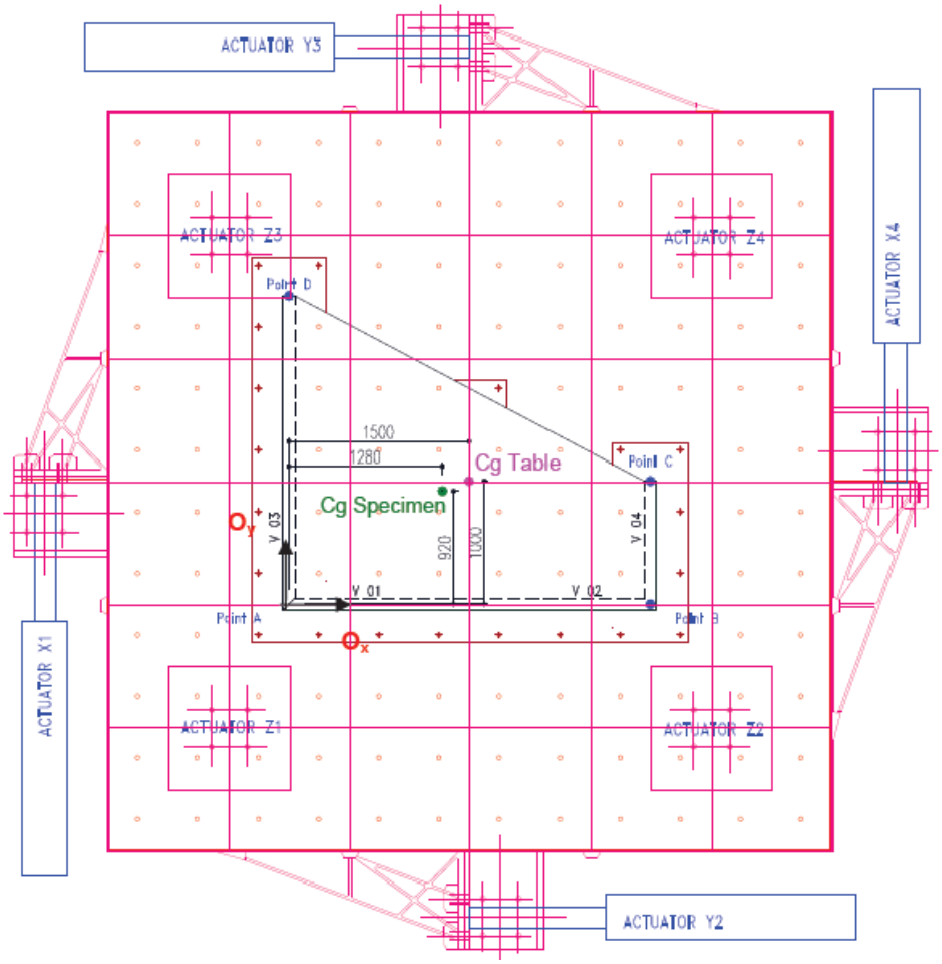

Figure 8: Positioning the superstructure on the Azalee table

3.2 FEM MODEL

Every participant at the SMART 2013 benchmark was asked to build a numerical model to carry on with the seismic analyses, recreating the benchmark mockup previously described.

The purpose of the project is to obtain realistic and accurate information about how the structure reacts to seismic loadings, in terms of local displacements and damage and this is why it's necessary to work with the non-simplified geometric numerical model described in the following chapter, and with a local approach in the material law (chapter 3.3.2).

3.2.1 SUPERSTRUCTURE

For obtaining a realistic and exhaustive model of the mockup it has been chosen to model it mainly with 3D 8-nodes cubic elements with linear interpolation shape functions.
In order to contain the computational cost of the program, this choice is applied only to the RC walls, to the central column and to the foundation letting easily identify the damaged zones and displaying an accurate displacements field.
Concerning the reinforcement steel bars (fig. 9), they've been modeled by beam elements: due to their geometry, an uniaxial element is well fitting the bars behavior.

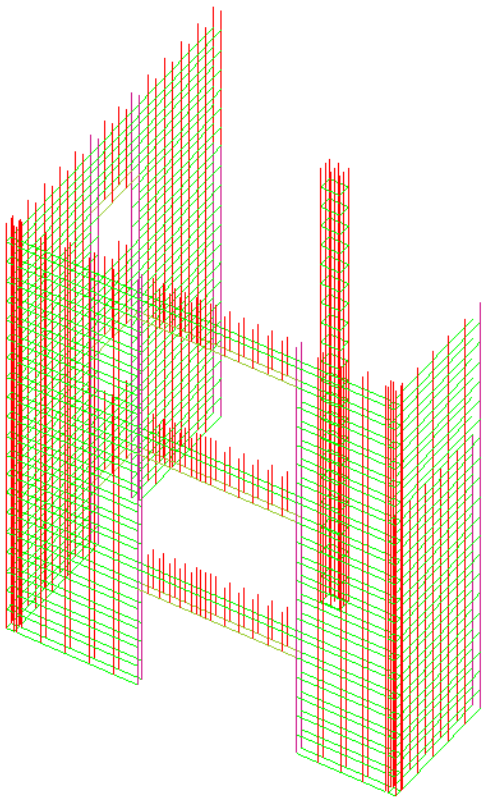

Figure 9: reinforcement steel bars

For the floor diaphragms, elastic shell elements are adopted because they won't be damaged by horizontal forces and they don't even need a nonlinear behavior law for the material.

A particular attention is given to the definition of the 5 reference points situated at each level (fig. 10) because the results are required in terms of displacement, speed and acceleration at these points.

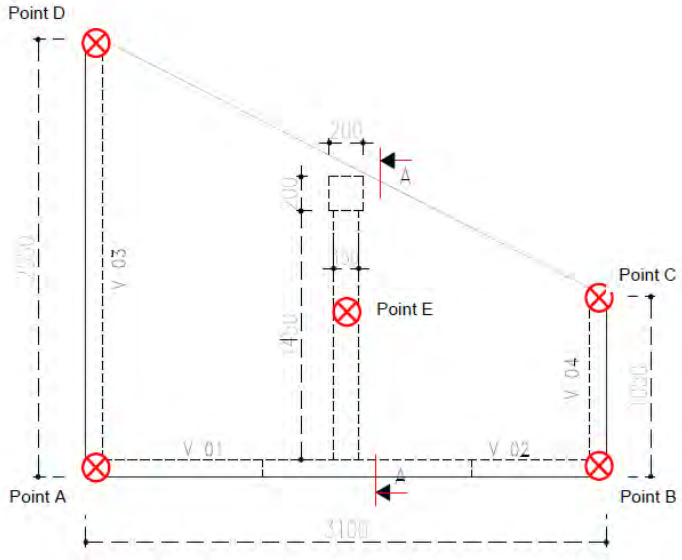

Figure 10: Reference points

The additional masses anchored at each floor for the reason previously described have been modeled by augmenting the mass density of the concrete horizontal slabs.

3.2.2 SHAKING TABLE

The Azalee shaking table has also been taken in account due to here influence in the seismic behavior of the building (Lermitte, 2008). The CEA provided a model made up of 4 node shell elements with a linear elastic constitutive law (Chaudat & Richard, 2013).

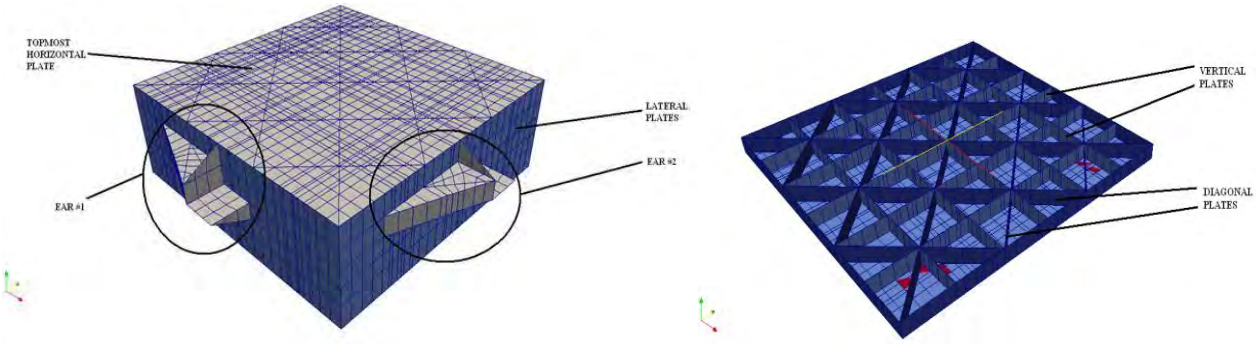

Figure 11: Shaking table CEA plates model

3.2.3 ASSEMBLY AND BOUNDARY CONDITIONS

The superstructure is assembled to the shaking table model through associating the its stiffness to the shaking table one, by forcing the first mesh points to follow a linear combination of the displacements field of the corresponding points in the second mesh.

The boundary conditions consist in blocking displacements at the jacks level: 2 are blocked in the x direction, 2 in the y direction while all of them are blocked in the vertical direction z. It's important to underline that the seismic charge will be applied as a chain of imposed displacements to these boundaries conditions.

After calculating the dead load of the mock-up and having defined the Ryleigh damping evolution, the nonlinear dynamic analysis is launched whit the PASAPAS procedure (chapter 3.5).

3.3 MODAL ANALYSIS AND ELASTIC CALIBRATION

In order to validate the assumptions made with the numerical model, a modal analysis and an elastic calibration have been undergone.

During the modal analysis, three different models were considered:

- Empty superstructure without the shaking table, directly anchored at foundations level (fig. 12);
- Corrected density superstructure without the shaking table;
- Corrected density superstructure assembled to the shaking table (fig. 13);

and the results were then compared to the experimental ones (fig. 14).

It stands out that taking in account the shaking table has a non-completely negligible influence in the seismic behavior of the building: the eigen frequencies are much more similar to the experimental ones when considering both the additional masses and the table.

The remarkable influence of the shaking table could be explained considering that the mock-up is a very rigid structure, which stiffness is almost comparable to the shaking table one.

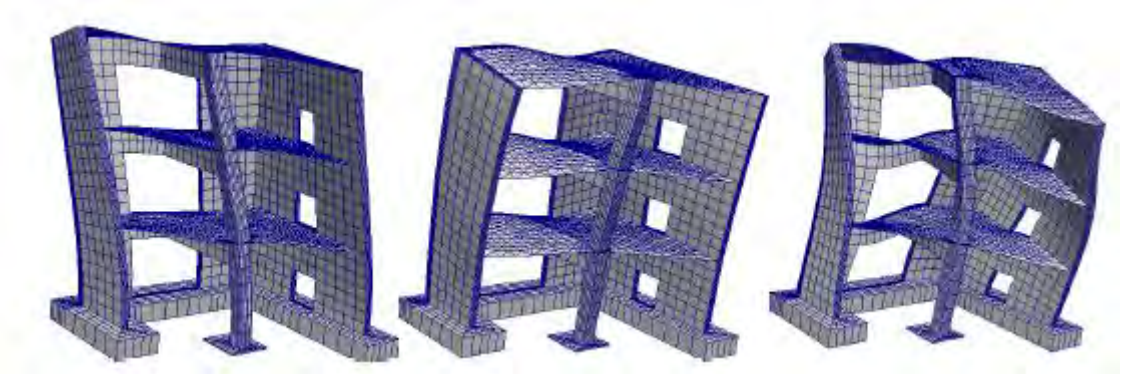

Figure 12: empty superstructure modes 1 (20,62 Hz), 2 (37,16 Hz) and 3 (66,80 Hz)

Figure 13: complete model modes 1 (6,23 Hz), 2 (10,28 Hz) and 3 (18,76 Hz)

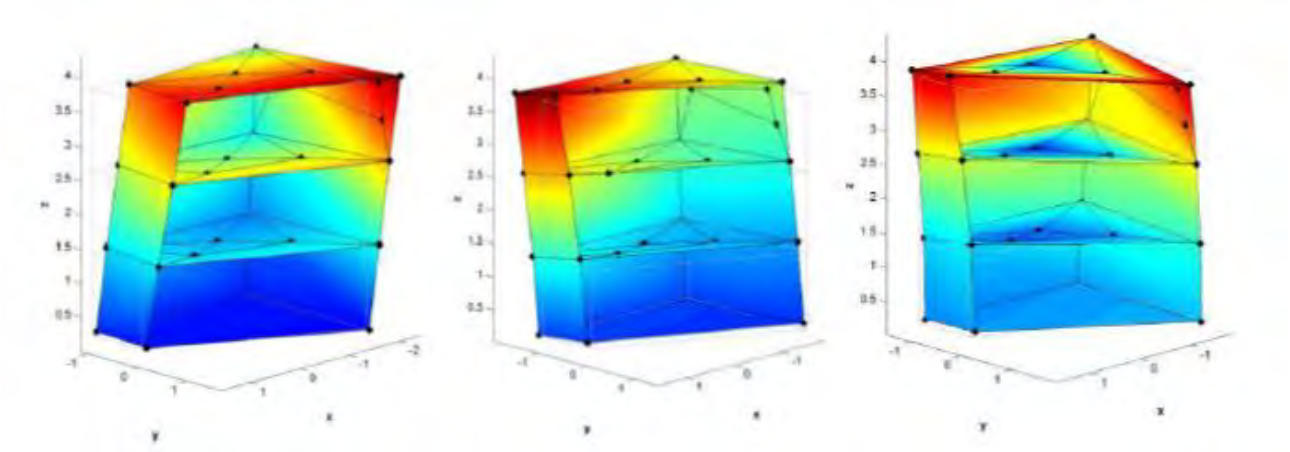

Figure 14: experimental modes 1 (6,28 Hz), 2 (7,86 Hz) and 3 (16,5 Hz)

The elastic calibration consisted in imposing a light seismic input (0,1g) to the numerical and compare the results to the experimental ones in terms of displacements, speed and acceleration at the 5 points level (RUN#6). As it could be noticed in fig. 15 and 16, there's not a remarkable difference between the two temporal evolutions and the elastic parameters values (young modulus..) could be considered appropriate.

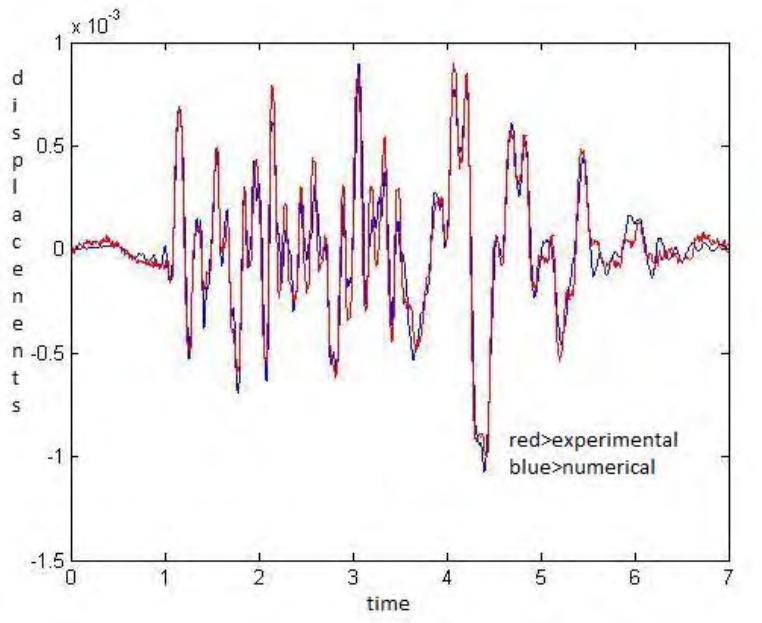

Figure 15: displacements evolution at point A 2nd floor

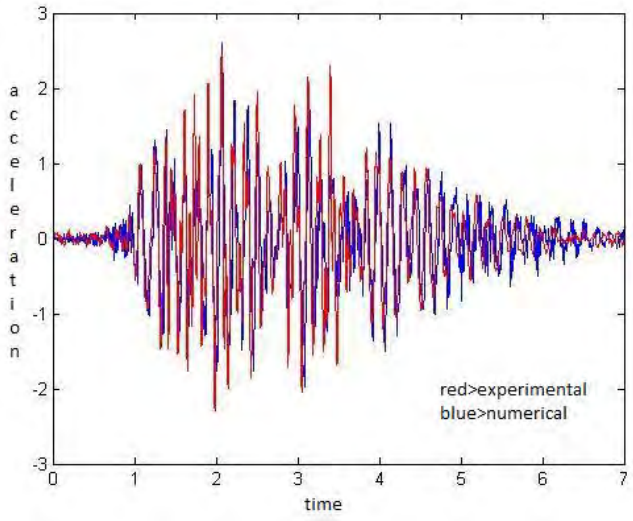

Figure 16: acceleration evolution at point D 2nd floor

For performing seismic analyses, it is necessary to define a damping value and it's possible to choose between:

- A simplified linear combination of the mass and stiffness matrix (Rayleigh damping matrix)

$$C = \alpha M + \beta K,$$

where α and β are two scalar coefficients, depending on the fist eigen frequencies,

$$\alpha = \frac{2\zeta}{2\pi(f_1+f_2)}, \quad \beta = \frac{2\pi}{2f_1 f_2 \alpha}$$

In this case, K and M are referred to the initial conditions and don't take in account any changes during the earthquake.

- More realistic could be considering the tangent stiffness matrix K^t ($C = \alpha M + \beta K^t$), accounting the stiffness variation during the dynamic phenomenon. Notice that in case of elastic domain, $K=K^t$
- The closest formulation to the real damping evolution, would consider the step-by-step update of the coefficients α and β, together with considering the tangent stiffness matrix K^t:

$$C = \alpha(t)M + \beta(t)K^t$$

Because of the increasing computational cost required by updating the eigen frequencies f_1 and f_2, or the stiffness matrix at every step of charge (Grégory, 2011), it has been chosen to work with the simplest linear combination described, even if this definition of the value leads to an overestimation of the damping, when not taking in account contribution of the internal sliding (Lemaitre, Chaboche, Benallal, & Desmorat, 2009) and the loss of stiffness due to damage (Zareiana & Medina, A practical method for proper modeling of structural damping in inelastic plane structural systems, 2009). In this case of study, it was suggest to take a damping value around 5% (coming out from measurements conducted during SMART 2008) and in particular the values used are:

- ζ=0.04
- f_1=6.23 Hz
- f_2=10,28 Hz.

3.4 MATERIAL LAWS

When strong seismic events affect buildings, it can be observed that materials are overcoming the linear range in their constitutive law and damage and plasticization take place: that's why it was necessary to introduce at this point of the project materials constitutive relations describing post-elastic phenomena and non linearities.

3.4.1 STEEL

Uniaxial constitutive laws for metal are generally showing a linear elastic part and then a hardening behavior till breaking point.

The steel is used in reinforced concrete as bars and it makes considering an uniaxial law adequate so that the Menegotto-Pinto model could well fit the steel behavior (Menegotto & Pinto, 1973).

3.4.1.1 THEORETICAL MODEL

For a monotonic loading, the relationship between stresses and strain could be divided in three phases: linear elasticity until $(\varepsilon_{sy}, \sigma_{sy})$ is reached, a plastic constant part $(\sigma = \sigma_{sy})$ followed by hardening behavior up to the point $(\varepsilon_{su}, \sigma_{su})$. The stress for $\varepsilon > \varepsilon_{sh}$ is written as:

$$\sigma = \sigma_{su} - (\sigma_{su} - \sigma_{sy}) \left(\frac{\varepsilon_{su} - \varepsilon}{\varepsilon_{su} - \varepsilon_{sh}} \right)^4 \qquad \textit{eq. 1}$$

When passing to a cyclic loading, the hardening becomes cinematic and the Bauschinger effect has to be represented. The hardening part inclination could be expressed as

$$E_h = \frac{\sigma_{su} - \sigma_{sy}}{\varepsilon_{su} - \varepsilon_{sy}} \qquad \textit{eq. 2}$$

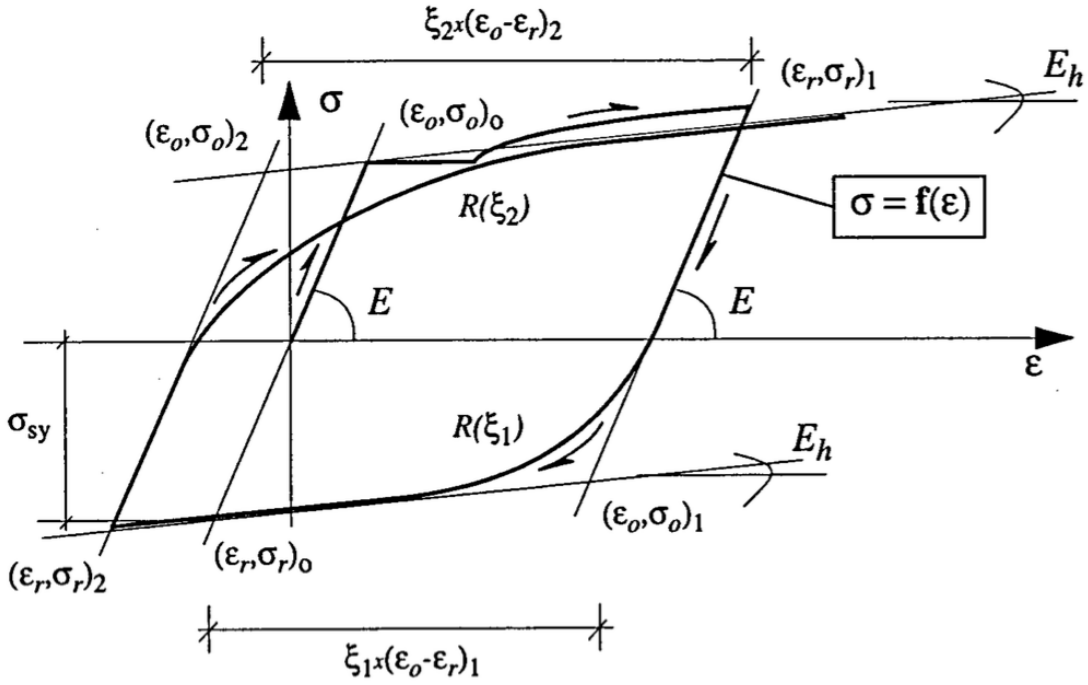

Figure 17: steel constitutive law

3.4.1.2 CASTEM MODEL

This constitutive law is implemented in Cast3m under ACIER_UNI (Combescure, 2001)and it has been slightly modified in order to take in account the buckling phenomenon in cyclic loading.

3.4.1.3 PARAMETER VALUES

In the SMART 2013 benchmark, the participants are asked to provide the results in terms of stresses and strains of a model of the chosen steel law applied to a 1m bar submitted to cyclic loading.

Some of the steel parameters were prescribed by the CEA, as for Young modulus, Poisson ratio, yield stress and ultimate stress, while the others have been chosen following Cast3m suggestions (Di Paola, 2001).

Table 4: steel parameters values

Properties	Variables	Values
Young Modulus E [Pa]	YOUN	200E9
Density ρ [kg/cm^3]	RHO	7800
Poisson's coeff. N	NU	0.3
Yield stress [MPa]	STSY	500E6
Strain at beginning of hardening [cm]	EPSH	2.3E-2
Ultimate stress [MPa]	STSU	600E6
Ultimate strain [cm]	EPSU	9.8E-2
Lshear/diameter	FALD	4.9
Coeff A6	A6FA	620
Coeff C	CFAC	0.5
Coeff A	AFAC	0.008
Coeff R0	ROFA	20
Ratio Kcyclic/Kelastic	BFAC	0.0116
Coeff A1	A1FA	18.5
Coeff A2	A2FA	0.15

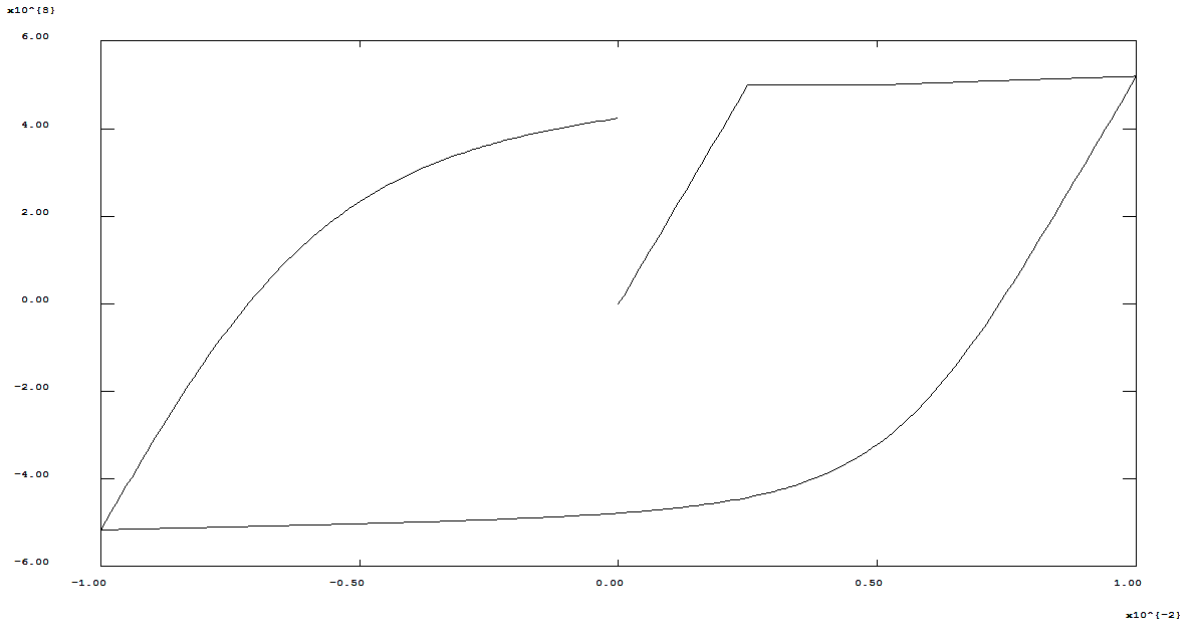

Figure 18: cyclic steel behavior with ACIER_UNI

3.4.2 CONCRETE

The constitutive laws for rocks and similar materials are generally characterized by an asymmetric behavior in tension and compression. In particular, for the tension range, the stress-strain relation shows a fragile trend, with almost instantaneous rupture even for low values, while for the compression range, the trend passes from a linear elastic behavior to a softening trend, till breaking point.

When analyzing the cyclic behavior of this material, many local phenomena are found out to influence the stress-strain trend, such as micro-cracking and internal sliding, and one of the best ways of representing all of it, is to opt for a continuum-damage-mechanics-based method, founded on the formulation of a thermodynamic potential.

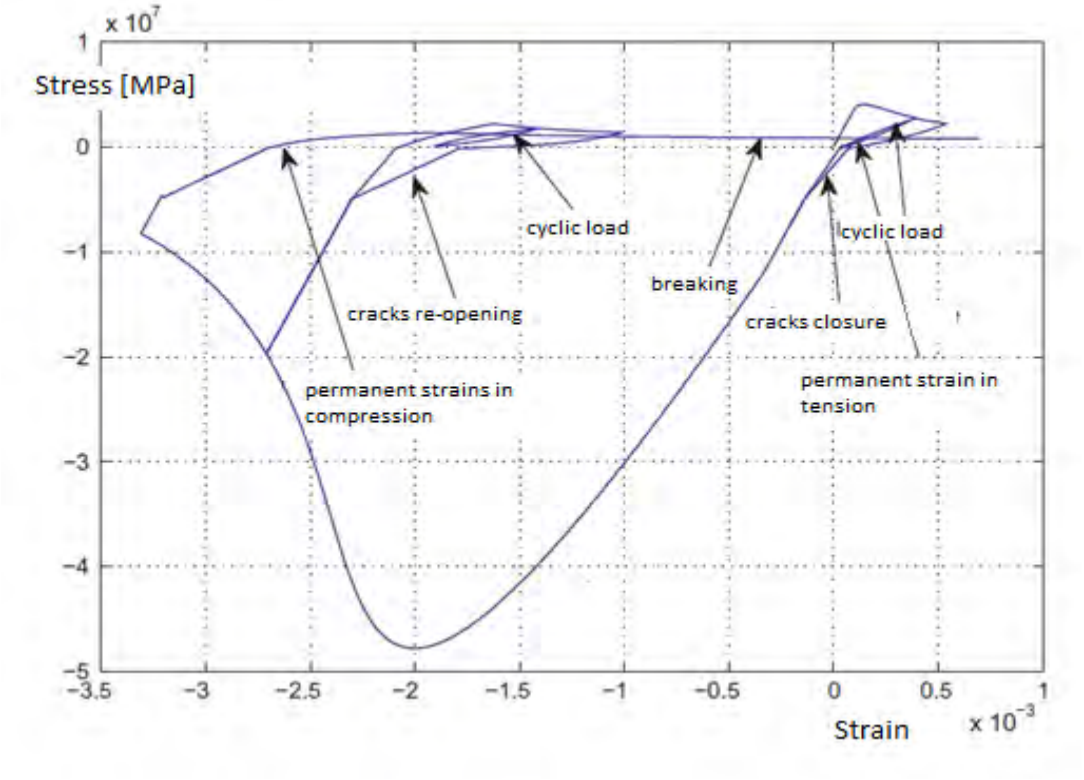

Figure 19: Concrete stress-strain relation in cyclic loading

3.4.2.1 THEORETICAL MODEL

The Ricbet model chosen to fit concrete brittle behavior and cyclic loading is capable of coupling damage, unilateral effect and friction.

Peculiarities of this model are that the unilateral effect is taken in account by introducing a closure function so that full stiffness is recovered when passing from tension to compression and nonlinearities in compression are not described by damage but by plasticity.

Starting from the theory of irreversible thermodynamic process, the thermodynamic potential is chosen as :

$$\rho\psi = \frac{1}{2}\{(1-d)(\varepsilon_{ij}-\varepsilon_{ij}^{p})C_{ijkl}(\varepsilon_{kl}-\varepsilon_{kl}^{p}) + d(\varepsilon_{ij}-\eta\varepsilon_{ij}^{\pi}-\varepsilon_{ij}^{p})C_{ijkl}(\varepsilon_{kl}-\eta\varepsilon_{kl}^{\pi}-\varepsilon_{kl}^{p}) + \gamma\alpha_{ij}\alpha_{ij}\} + H(z) + G(p)$$

Where:

d=scalar damage variable

ε=strain tensor

p=plasticity

π=internal sliding

C=Hook tensor

η=crack closure variable

γ=kinematic hardening modulus

α=kinematic hardening tensor

H=consolidation function in tension

G=consolidation function in compression

One can notice that the potential is divided in two parts: one driving the elastic-plastic damage and the other concerning the internal sliding.

State equations

By differentiating the state potential, the reversible part of the mechanical behavior can be obtained:

- Cauchy stress

$$\sigma_{ij} = \frac{\partial \rho\psi}{\partial \varepsilon_{ij}} = \frac{-\partial \rho\psi}{\partial \varepsilon_{ij}^{p}} = (1-d)C_{ijkl}\left(\varepsilon_{kl} - \varepsilon_{kl}^{p}\right) + dC_{ijkl}\left(\varepsilon_{ij} - \eta\varepsilon_{ij}^{\pi} - \varepsilon_{ij}^{p}\right)$$

- tangent modulus D_{ijkl}

$$D_{ijkl} = \frac{\partial \sigma_{ij}}{\partial \varepsilon_{kl}} = C_{ijkl}$$

- sliding stress

$$\sigma_{ij}^{\pi} = \frac{\partial \rho\psi}{\partial \varepsilon_{ij}^{\pi}} = \eta d C_{ijkl}\left(\varepsilon_{kl} - \eta\varepsilon_{kl}^{\pi} - \varepsilon_{kl}^{p}\right)$$

- energy rate released by the damage mechanism

$$Y = \frac{-\partial \rho\psi}{\partial d} = \frac{1}{2}\left\{\left(\varepsilon_{ij} - \varepsilon_{ij}^{p}\right)C_{ijkl}\left(\varepsilon_{kl} - \varepsilon_{kl}^{p}\right) - \left(\varepsilon_{ij} - \eta\varepsilon_{ij}^{\pi} - \varepsilon_{ij}^{p}\right)C_{ijkl}\left(\varepsilon_{kl} - \eta\varepsilon_{kl}^{\pi} - \varepsilon_{kl}^{p}\right)\right\}$$

- thermodynamic force associated with isotropic hardening

$$Z = \frac{\partial \rho\psi}{\partial z} = \frac{dH(z)}{dz}$$

- back stress

$$X_{ij} = \frac{\partial \rho\psi}{\partial \alpha_{ij}} = \gamma\alpha_{ij}$$

- thermodynamic force associated with the closure variable

$$\zeta = \frac{-\partial \rho\psi}{\partial \eta} = d\varepsilon_{ij}^{\pi} C_{ijkl}\left(\varepsilon_{kl} - \eta\varepsilon_{kl}^{\pi} - \varepsilon_{kl}^{p}\right)$$

- thermodynamic force associated with the plastic hardening

$$R = \frac{\partial \rho\psi}{\partial p} = \frac{dG(p)}{dp}$$

Flow rules

The flow rules describe three separate threshold surfaces:

1. *Damage and isotropic hardening*

The threshold surface is:

$$f_d = \bar{Y} - (Y_0 + Z) \geq 0$$

The link between damage and positive extensions is due to assuming cracked behavior separable into two independent behaviors: cracks opening and closing are considered through the hydrostatic strain part of the model while the frictional sliding is modeled by the deviatoric part of the strain and stress tensors. The flow rules can be written starting from normality rules:

$$\dot{d} = \dot{\lambda_d} \frac{\partial f_d}{\partial \bar{Y}} = \dot{\lambda_d}$$

$$\dot{z} = \dot{\lambda_d} \frac{\partial f_d}{\partial z} = -\dot{\lambda_d}$$

In order to compute the Lagrange multiplier explicitly, thanks to the consistency condition $f_d = \dot{f_d} = 0$, a consolidation function H(z) has to be chosen from which the following expressions can be obtained:

$$d = 1 - \frac{1}{1 + A_d(\bar{Y} - Y_0)}$$

$$z + d = 0$$

2. *Internal sliding and kinematic hardening*

The threshold surface is a function of sliding stress and back stress and there's no initial threshold in order to activate the mechanism only when damage overcomes.

$$f_\pi = \sqrt{\frac{3}{2}\left(\sigma_{ij}^\pi - X_{ij}\right)\left(\sigma_{ij}^\pi - X_{ij}\right)} H(\sigma_{kk}) \leq 0$$

To take in account the non-linearities managed by hysteretic effects a pseudo potential is chosen as follows:

$$\phi_\pi = \sqrt{\frac{3}{2}\left(\sigma_{ij}^\pi - X_{ij}\right)\left(\sigma_{ij}^\pi - X_{ij}\right)} + \frac{a}{2} X_{ij} X_{ij}$$

And the flow rules:

$$\dot{\varepsilon_{ij}^\pi} = \dot{\lambda_\pi} \frac{\partial \phi_\pi}{\partial \sigma_{ij}^\pi}$$

$$\dot{\alpha_{ij}} = -\dot{\lambda_\pi} \frac{\partial \phi_\pi}{\partial X_{ij}}$$

Unilateral effect

This effects can be defined as the stiffness recovering when switching from tension to compression, up to the initial undamaged one, due to the crack closure following the linear rule $\eta = 1 - \frac{\sigma_{kk}}{\sigma_f}$.

3. Plasticity and isotropic hardening

threshold function has been chosen as a Drucker–Prager criterion and it provides a satisfying description of the dilatancy

$$f_p = \left(\sqrt{\frac{3}{2}\sigma_{ij}\sigma_{ij}} + \alpha_{f_p}\frac{1}{3}\sigma_{kk}H\left(\sigma_f - \sigma_{kk}\right) - (R + f_c) \right) \geq 0$$

Where the isotropic hardening variable is $R(p) = (a_r p + f_c)exp(-b_r p) - f_c + \sigma_f$.

It's to note that when plasticity is activated, the internal sliding has no effects cause the closure function is null.

The pseudo-potential and the normality rules are:

$$\phi_p = \left(\sqrt{\frac{3}{2}\sigma_{ij}\sigma_{ij}} + \alpha_{\phi_p}\frac{1}{3}\sigma_{kk} - (R + f_c) \right) \geq 0$$

$$\dot{\varepsilon_{ij}^p} = \dot{\lambda_p}\frac{\partial \phi_p}{\partial \sigma_{ij}}$$

$$\dot{p} = -\dot{\lambda_p}\frac{\partial \phi_p}{\partial R}$$

In order to fulfill the consistency condition $f_p = \dot{f_p} = 0$ the flow rules have to be implicitly integrated with a return-mapping algorithm.

Thanks to this constitutive law, one is able to represent the major local phenomena characterizing concrete when cyclically loaded, as demonstrate in the following sections.

3.4.2.2 REGULARIZATION

Brittle materials presents a typical softening behavior which, in the classical local fe methods leads to mesh dependency: when cracks start spreading, the resistant net area decreases and stresses localize. Moreover if the energy rate released by damage is

considered finite per unit of volume, and the element dimension tends to 0, the structure is supposed to fail at zero energy dissipation.

In order to avoid the mesh dependence problems occurring in continuum damage mechanics based models, a nonlocal approaches have been investigated (Pijiaudier-Cabot & Bazant, 1987)

The ellipticity of local equilibrium equations is often lost when considering micro cracked elements or next to boundaries ones (Giry, Dufour, & Mazars, 2011). The principle of energy balance approach is to assume that a certain amount of energy is absorbed by the formation of a unit area of crack surface and the crack propagates when the released energy is greater than the stored one.

In particularly in Hillerborg regularization approach (Hillerborg, Modéer, & Peterson) the crack is supposed to propagate when the tensile strength f_t is reached at the tip of the crack, then the stress fall down following a function of the width w (when $w=w_1$ the stress is back to zero).

The energy stored in order to open the crack up to w_1 is

$$G_c = \int_0^{w_1} \sigma dw$$

per unity of cracked area, where the function $\sigma(w)$ could be chosen properly for each material.

Concerning to the Ricbet model, the local energy rate released by damage is $\bar{Y}$ and it's averaged over a given l_c (3 or 4 times the aggregate size) vicinity , centered in the current Gauss' point *x,* thanks to a weight function $\Omega(x)$:

$$\bar{Y}^{nl} = \frac{\int_{\Omega(x)} \bar{Y}(x)\omega(x-s)ds}{\int_{\Omega(x-s)} \omega(s)ds}$$

f_d becomes $f_d^{nl}$and the damage variable is rewritten.

This procedure has been chosen because it just requires the substitution of the local variable of energy rate released due to damage with an averaged one and it's not increasing the computational cost.

3.4.2.3 CASTEM MODEL

The numerical implementation lies in calculating the stress increment knowing the thermodynamic state of the material at a given step (*i*).

After giving the fixed strain increment, the numerical scheme calculates and updates all the internal variables and the corresponding forces.

The flow rules associated with damage are explicitly integrated, the internal sliding and the plasticity mechanisms are treated thanks to a return mapping-based algorithm.

First of all, the variables are initialized and the thermodynamic state is given.

- Damage and isotropic hardening

damage is linked to positive strain so the positive part of the total strain tensor is extracted and then the threshold surface is tested, after calculating the energy rate Y_P. If $f_d^{i+1} < 0$, $\Delta d = 0$, then $\Delta d \neq 0$ and the damage variable is updated:

$$d^{i+1} = 1 - \left(\frac{f_t}{E\bar{Y}}\right) exp\left[A_d\left(\frac{f_t}{E} - \bar{Y}\right)\right]$$

and also

$$Z^{i+1} = \bar{Y}^{i+1} - Y_0$$

One have to notice that the expressions for *Y* and *d* have been changed because of the choice of working whit an energy regularized version.

- Internal sliding and kinematic hardening

Following the return mapping-based algorithm procedure, an elastic prediction of the sliding stress tensor is made

$$\sigma_{ij}^{\pi,i+1,trial} = d^{i+1} C_{ijkl}\left(\varepsilon_{kl}^{i+1} - \varepsilon_{kl}^{\pi,i} - \varepsilon_{kl}^{p,i}\right)$$

If the postulated threshold surface is positive ($\sigma_{kk} > 0$) $\Delta\varepsilon_{ij}^{\pi,i} \neq 0$ and it's linearized as follows:

$$f_\pi^{i+1,k+1} = f_\pi^{i+1,k} - d^{i+1}\frac{\partial f_\pi^{i+1,k}}{\partial \sigma_{ij}^{\pi,i,k}} C_{ijkl} \frac{\partial f_\pi^{i+1,k}}{\partial \sigma_{ij}^{\pi,i,k}} \Delta\lambda_\pi^k - \gamma \frac{\partial f_\pi^{i+1,k}}{\partial X_{ij}^{i,k}} \frac{\partial \phi_\pi^{i+1,k}}{\partial X_{ij}^{i,k}} \Delta\lambda_\pi^k \approx 0$$

The Lagrange multiplier, the sliding stress and the back stress increments can be computed as:

$$\Delta\lambda_\pi^k = \frac{f_\pi^{i+1,k}}{d^{i+1}\frac{\partial f_\pi^{i+1,k}}{\partial \sigma_{ij}^{\pi,i,k}} C_{ijkl} \frac{\partial f_\pi^{i+1,k}}{\partial \sigma_{kl}^{\pi,i,k}} + \gamma \frac{\partial f_\pi^{i+1,k}}{\partial X_{ij}^{i,k}} \frac{\partial \phi_\pi^{i+1,k}}{\partial X_{ij}^{i,k}}}$$

$$\Delta\sigma_{ij}^{\pi,i,k} - d^{i+1}\Delta\lambda_\pi^k C_{ijkl} \frac{\partial f_\pi^{i+1,k}}{\partial \sigma_{ij}^{\pi,i,k}}$$

$$\Delta X_{ij}^{\pi,i,k} = -\gamma\Delta\lambda_\pi^k \frac{\partial \phi_\pi^{i+1,k}}{\partial X_{ij}^{i,k}}$$

And finally the sliding stress and the back stress tensors can be updated until

$$\frac{f_\pi^{i+1,k+1}}{f_\pi^{i+1,0}} < 10^{-8}$$

- Unilateral effect

The closure function depends on σ_{kk} and σ_f following a linear law. When the case $\sigma_{kk} \leq \sigma_f \leq 0$ overcomes, by using the stress-strain relation projected on the hydrostatic basis the following expression is obtained

$$\sigma_{kk}^{i+1} = \frac{k\left(\varepsilon_{kk}^{i+1} - \varepsilon_{kk}^{\pi,i+1} - \varepsilon_{kk}^{p,i+1}\right)}{1 - \frac{k}{\sigma_f}\varepsilon_{kk}^{\pi,i+1}}$$

And the updated Cauchy stress is then computed and updated:

$$\sigma_{ij}^{i+1} = \frac{1}{3}\sigma_{kk}^{i+1}\delta_{ij} + \sigma_{ij}^{d,i+1}$$

- Plasticity and isotropic hardening

Once again the variables are integrated thanks to a return mapping algorithm: an elastic prediction of the Cauchy stress is made, where no internal sliding parameters are shown because of the closed cracks state.

$$\sigma_{ij}^{i+1,trial} = d^{i+1}C_{ijkl}\left(\varepsilon_{kl}^{i+1} - \varepsilon_{kl}^{p,i}\right)$$

The threshold surface is then calculated and if $f_p^{i+1} > 0$ then $\Delta\varepsilon_{ij}^p \neq 0$ and f_p is linearized and the variables are updated till stop criterion is reached (Richard B. , Ragueneau, Cremona, & Adelaide, 2010).

As fig. 20 shows, the numerical stress-strain relation is well fitting the experimental one.

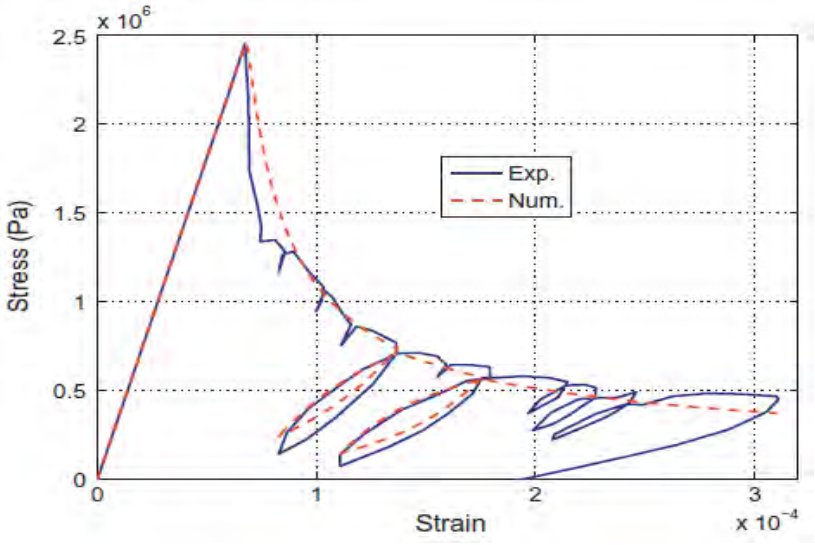

Figure 20: Numerical and experimental trends of a concrete sample under cyclic loading

3.4.2.4 PARAMETER VALUES

At the end of the SMART 2008 campaign it stood out how scattered were the results of the different participants and it was also due to the large variability of the parameters value used (see for example the value of Young modulus in fig. 21).

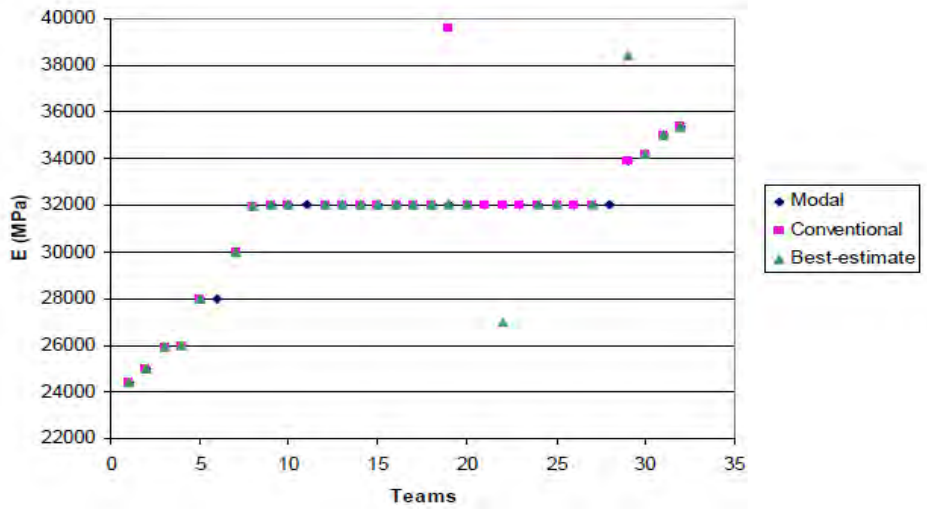

Figure 21: Young modulus variability in SMART 2008

As a consequence of that, the organizing committee decided to prescribe the value of some of the concrete properties as Young modulus, Poisson ratio, fracture energy…(annex 2).

Concerning the other parameters, they are suggested by experimental and numerical experience and they've been resumed in table.

Table 5: concrete parameters values

Properties	**Variable**	**Values**
Young Modulus E	YOUN	Annex 3
Density ρ [kg/cm^3]	RHO	2300
Poisson's coeff. v	NU	0.2
Tensile strength	FT	Annex 3
Hardening modulus 1	GAM1	5.0E9
Hardening modulus 2	A1	8.0E-6
Closure stress [MPa]	SREF	-3.0E6
Brittleness in tension	ALDI	Depends on Lc and GF
Yield surface 1	AF	0.7

Yield surface 2	BF	0.3
Plastic potential 1	AG	0.6
Plastic potential 2	BG	0.45
Yield hardening 1	AC	2.52E10
Yield hardening 2	BC	700.0
Asymptotic stress in compression [MPa]	SIGU	-4.0E6 MPa
Initial compression strength [MPa]	FC	6.0E6 MPa
Fracture energy	GF	Annex 3

As for the steel parameters, the SMART 2013 project requires some simple tests on a concrete cube in order to verify the coherence of the values chosen, and the participants have to submit the results in terms of stress and strain.

Here are the diagrams (σ, ε) for the Ricbet model applied to the concrete object:

- Softening in tension

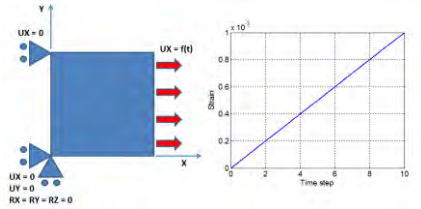

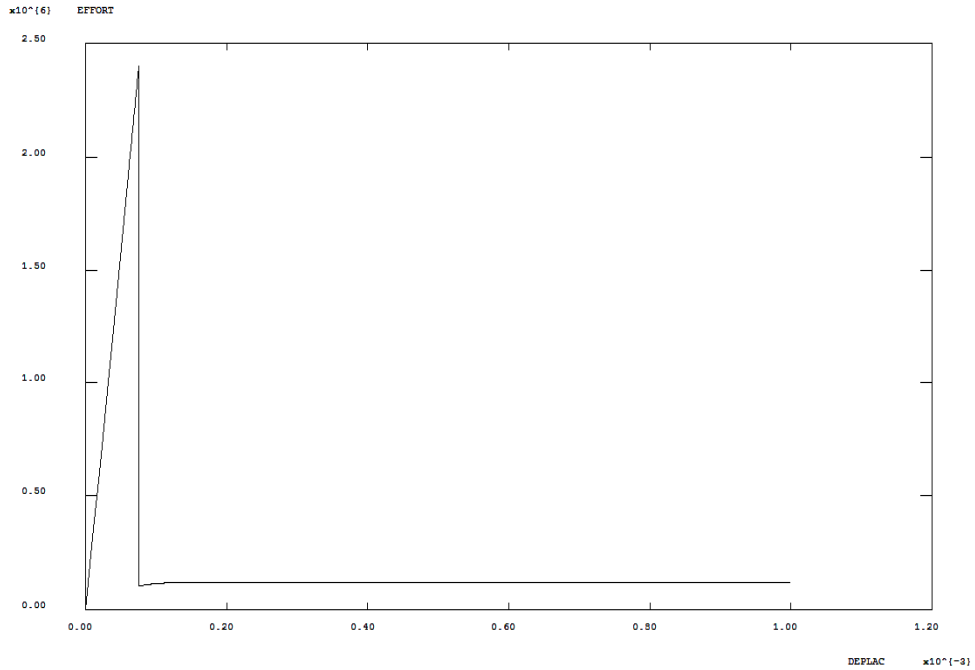

This simple traction test shows the material fragility in tension : the improvise fall of tension represents the instant rupture of the concrete cube, which is characteristic of brittle behavior.

- Softening in compression

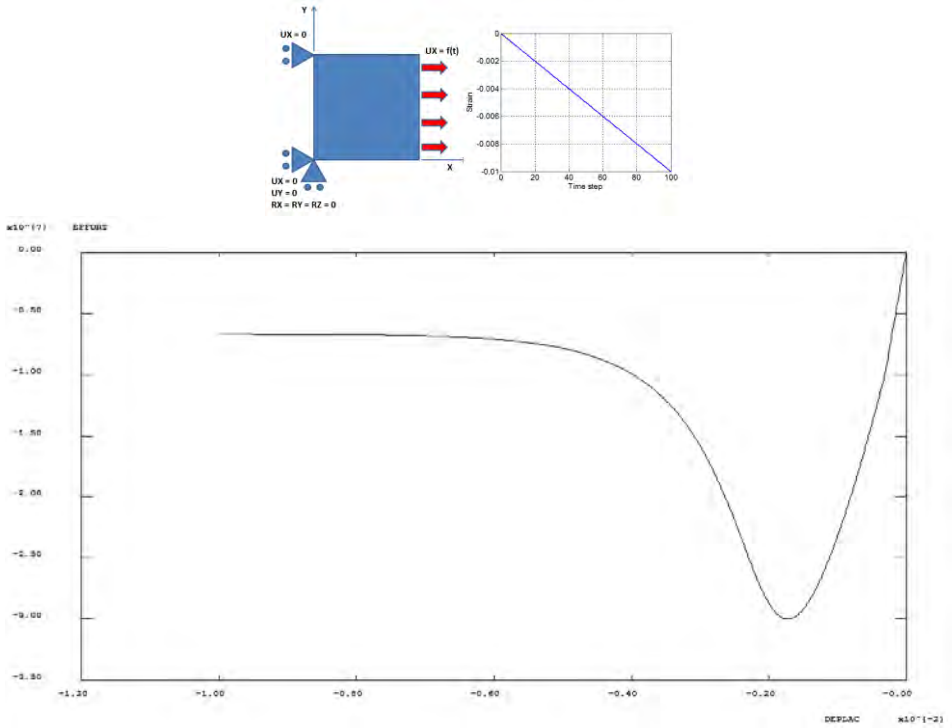

The shape of the compression curve is driven not by damage but by plasticity parameters.

- Cyclic response

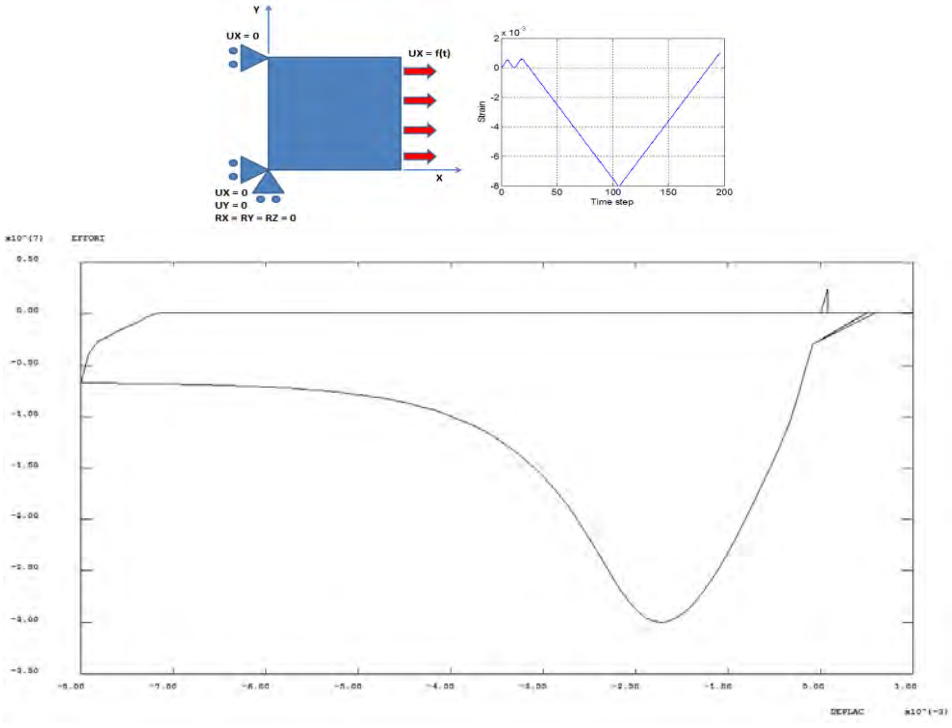

The cyclic test make evidence of the unilateral effect phenomena when compressing: the stiffness goes back to the initial value once the cracks are closed.

3.4.3 REINFORCED CONCRETE

Once again a small RC cube is tested and the model sensitivity to parameters is investigated, as requested by the Benchmark.

- Cyclic response, membrane part

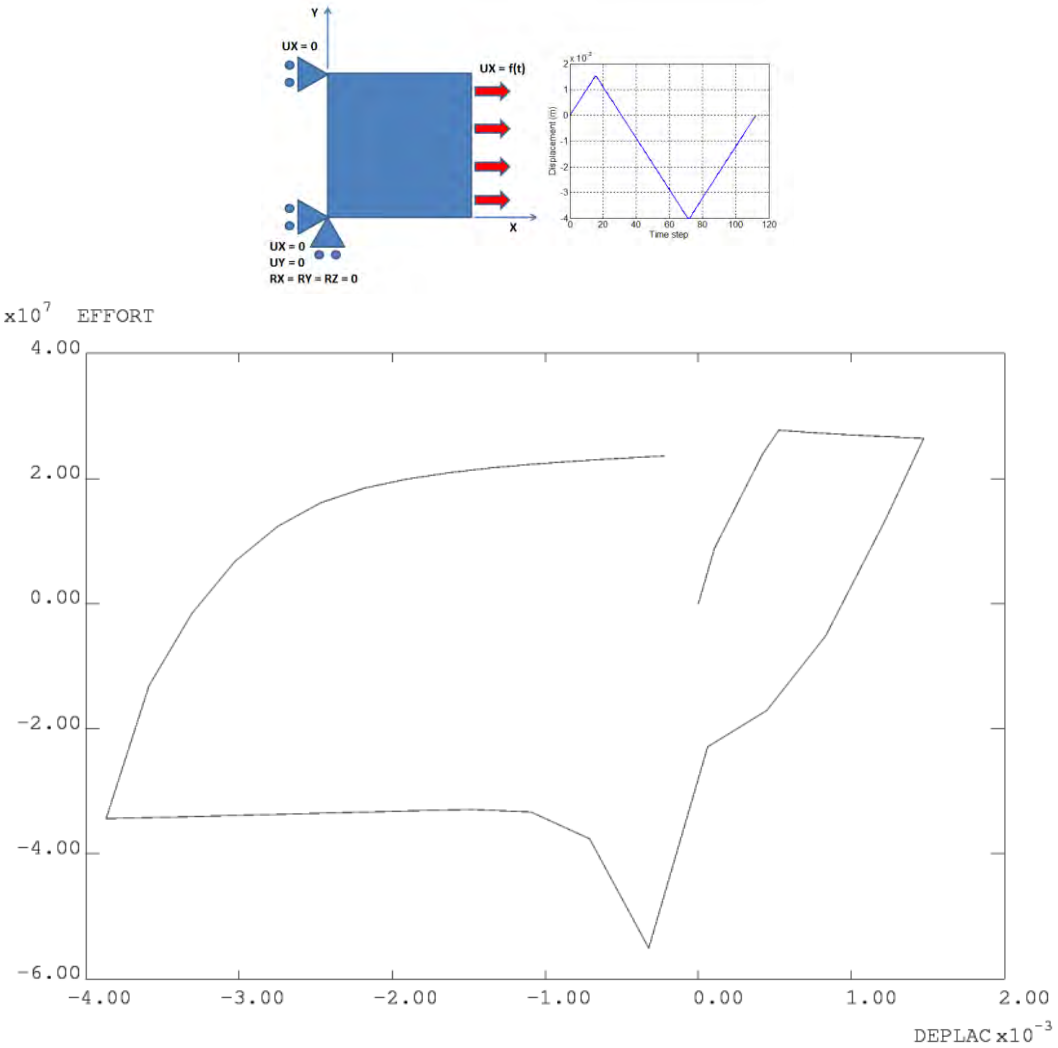

The traction part is behaving like steel properties while the compression is mainly driven by concrete parameters.

- Cyclic response, flexion part

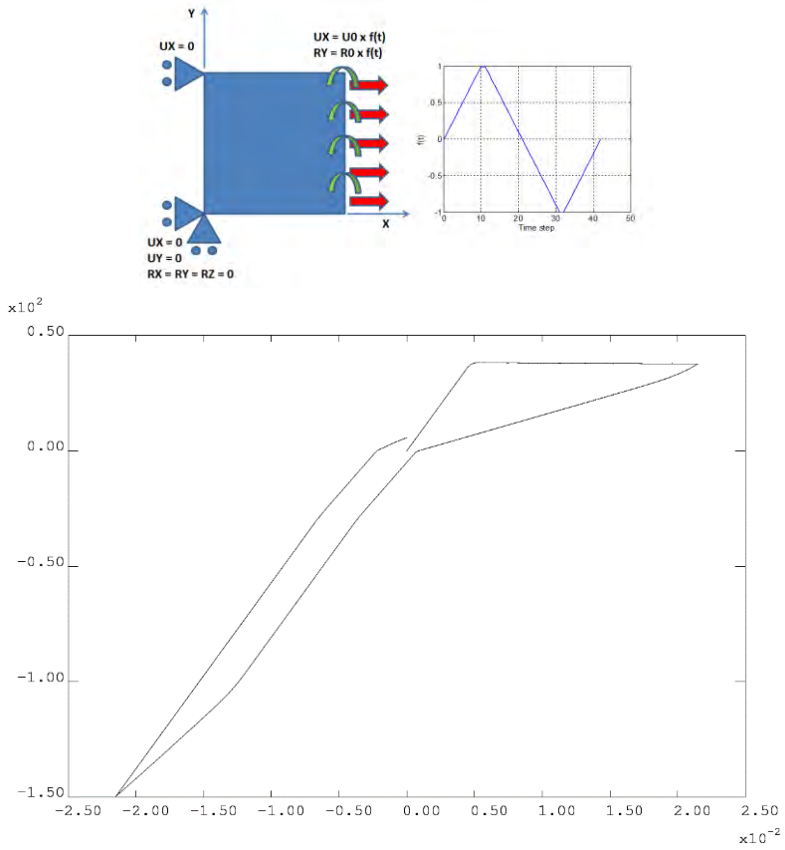

This test didn't make the cube reaching the peak value in compression so what could be seen is just an almost linear behavior.

3.5 TIME-HISTORY ANALYSIS

In the pursuance of coupling the non-linear constitutive law previously described for the concrete, and the complex structure response due to the high seismic inputs provided, it is necessary to carry on the most detailed type of analysis: the time-history analysis.

3.5.1 THEORY

With the finite elements method, the dynamic problem discretization is written as:

$$\underline{\underline{M}}\ddot{U} + \underline{\underline{C}}\dot{U} + B\underline{\underline{\sigma}} = \underline{F}$$

where σ are the elements stresses, F are the nodal forces and B the divergence operator, to be solved for each time step.

Passing to the weak form of the dynamic problem, after a spatial discretization, it becomes:

$$\begin{cases} given\ b\ ,t\ and\ \bar{u} \\ Find\ u\ so\ that,\ \forall\omega: \\ -\int_\Omega \bar{\bar{\sigma}}\colon \bar{\bar{\varepsilon}}(\bar{\omega})dV + \int_\Omega \bar{b}\,.\,\bar{\omega}\,dV + \int_{\partial\Omega} \bar{t}\,.\,\bar{\omega}\,dS = \int_\Omega \rho\,\bar{\gamma}.\bar{\omega}\ dV \end{cases}$$

Because of the great difficulties in finding an analytical solution to this system, numerical methods had been computed, as the Finite Elements Methods for example.

Proceeding to the spatial discretization, the local form of the real and virtual displacements could be written as:

$$\begin{cases} u^h(\zeta\ ,t) = \sum_{a=1}^{n_{elts}} N_a\ (\zeta)U_a(t) \\ w^h(\zeta\ ,t) = \sum_{a=1}^{n_{elts}} N_a\ (\zeta)W_a(t) \end{cases}$$

Where N_a represents the shape functions, U_a and W_a the nodal displacements, the real and virtual ones respectively.

By using isoparametric elements, the geometric interpolation is :

$$x^h(\zeta\ ,t) = \sum_{a=1}^{n_{elts}} N_a\ (\zeta)X_a$$

X_a representing the elementary element nodal coordinates

Knowing that :

$$B(\zeta) = \frac{dN_a(\zeta)}{d\zeta}\ J^{-1}(\zeta)$$

where $J^{-1}(\zeta)$ is the Jacobean matrix inverse, the strain field could be written as:

$$\varepsilon^h(\zeta\ ,t) = \sum_{a=1}^{n_{elts}} B_a\ (\zeta)U_a(t)$$

And the weak formulation becomes :

$$\Lambda_{e=1}^{n_{elts}}\left(f^{acc,e} + f^{int,e}\right) = \Lambda_{e=1}^{n_{elts}} f^{ext,e}$$

with $f^{acc,e}$, $f^{int,e}$ and $f^{ext,e}$ representing the acceleration forces, internal and external forces respectively.

The spatial form of the problem is finally reached:

$$\begin{cases} Find\ U(t)\ and\ \ddot{U}(t)\ so\ that: \\ \Lambda_{e=1}^{n_{elts}} M\ U(t) + \int_\Omega B^t\sigma(U)dV = \Lambda_{e=1}^{\ddot{n}_{elts}} \int_\Omega N^t b dV + \int_{\partial\Omega} N^t \bar{t} dS \end{cases}$$

Once written the problem under this form, a temporal integration scheme has to be defined, as for example the Newmark's one: this is strongly adapted to situations where nonlinear procedures appear and the forces are time or space-depending.

Starting from time steps t_n and t_{n+1}, speeds and displacements are computed :

$$\begin{cases} u_{n+1} = u_n + \Delta t\ v_n + \left(\frac{1}{2} - \beta\right)\Delta t^2 a_n + \beta\Delta t^2 a_{n+1} \\ v_{n+1} = v_n + (1-\gamma)\Delta t\ a_n + \gamma\Delta t\ a_{n+1} \end{cases}$$

where $\beta\ and\ \gamma$ are two parameters from which the stability and the implicit/explicit form of the algorithm are depending to.

Remember that in explicit algorithms, the state of the system at time step t_{n+1} depends only from the state at the previous step t_n, while in implicit algorithms the variables at t_{n+1} are depending both from the current and previous states.

As an example, by setting:

- $\gamma = 1/2$ and $\beta = 0$, an explicit and conditionally stable algorithm is obtained :

$$\begin{cases} u_{n+1} = u_n + \Delta t\, v_n + \frac{1}{2}\Delta t^2 a_n \\ v_{n+1} = v_n + \frac{1}{2}\Delta t\, (a_n + a_{n+1}) \end{cases}$$

- $\gamma = 1/2$ and $\beta = 1/4$, an implicit and unconditionally stable algorithm is obtained (average acceleration method) :

$$\begin{cases} u_{n+1} = u_n + \Delta t\, v_n + \dfrac{\Delta t^2}{4}(a_n + a_{n+1}) \\ v_{n+1} = v_n + \dfrac{\Delta t}{2}(\, a_n + a_{n+1}) \end{cases}$$

In general :

Domain	**Stability**
$\gamma \leq 1/2$	Instable
$1/2 \leq \gamma$ et $2\beta \leq \gamma$	Conditionally stable
$1/2 \leq \gamma$ et $\gamma \leq 2\,\beta$	Unconditionally stable

3.5.2 CASTEM (PASAPAS)

The nonlinear dynamic analysis is implemented in Cast3m with the PASAPAS procedure (Charras & Di Paola, 2011) and it's about the resolution of the Newmark algorithm with the method of mean accelerations, for which γ=1/2 and β=1/4 (implicit and unconditionally stable).

This procedure allows to charge the numerical model of the SMART 2013 mockup whit the real and detailed seismic inputs prescribed by the project, letting follow the evolution of the damage variable step by step.

The inputs are given under the form of time increments and respective displacements and they're applied to the hydraulics actuators corresponding points at the shaking table level.

For every step of time increment, a table (TAB1) containing the inputs is created:

- Model: containing the chain of all the objects describing the physic problem formulation, in this case it contains the geometric model of the structure and the elements type;

- Characteristics: object specifying the materials properties values, it means the type of constitutive law (Ricbet, Acier_uni) and the parameters illustrated in the previous chapters;
- Charges: object containing the temporal evolution of the boundaries conditions, it consists in a list of imposed displacements given by the seismic action;
- Times: object specifying the time steps.

At each time step, the procedure charges the structure starting from the previous results (saved in WTABLE) and gives the outputs in another table: common index as time, displacements, stresses, deformations (the numerical model presented has no thermic dependence), and some complementary information as errors, convergence, saved steps, added internal variables.

A general scheme of the procedure is reported in annex 3.

3.5.3 SEISMIC INPUTS

The seismic inputs are given to charge the table as vertical and horizontal displacements followed by yaw, roll and pitch inputs:

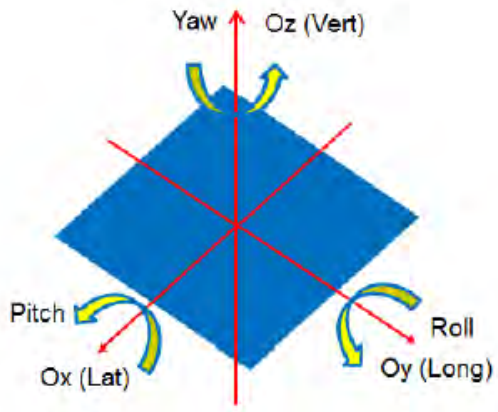

Figure 22: rotations

The displacements which are going to be imposed are calculated starting from those applied to the shaking table, combined also with given rotations, thanks to a Matlab filter:

DX1F = DYF - 3.305*RZF;

DX4F = DYF + 3.305*RZF;

DY2F = DXF + 3.305*RZF;

DY3F = DXF - 3.305*RZF;

DZ1F = DZF + 2.125*RYF - 2.125*RXF;

DZ2F = DZF + 2.125*RYF + 2.125*RXF;

DZ3F = DZF - 2.125*RYF + 2.125*RXF;

DZ4F = DZF - 2.125*RYF - 2.125*RXF;

Moreover the Matlab filter could also be useful for reducing the number of imposed steps when conducting preliminary calculations

The filtered results could then be applied to the boundary conditions: x2, x4, y1, y3 for horizontal directions and z1, z2, z3, z4 for vertical solicitations.

Because of the enormous number of time inputs provided for each run (10^4), the algorithm is initialized with the value of an increment filter set to 2, it means that the structure is charged each 2 displacement inputs.

The firsts imposed displacements considered (RUN#9) are referring to an earthquake of about 0.2g.

Secondly the whole structure had been submitted to the Northridge earthquake accelerogram (CA, 1994), leading to accelerations of about 1.7g.

Then it was considered also one of the Northridge earthquake aftershocks of about 0.2g again, but testing the already damaged building.

Here are reported some of the time-displacements prescribed by SMART 2013.

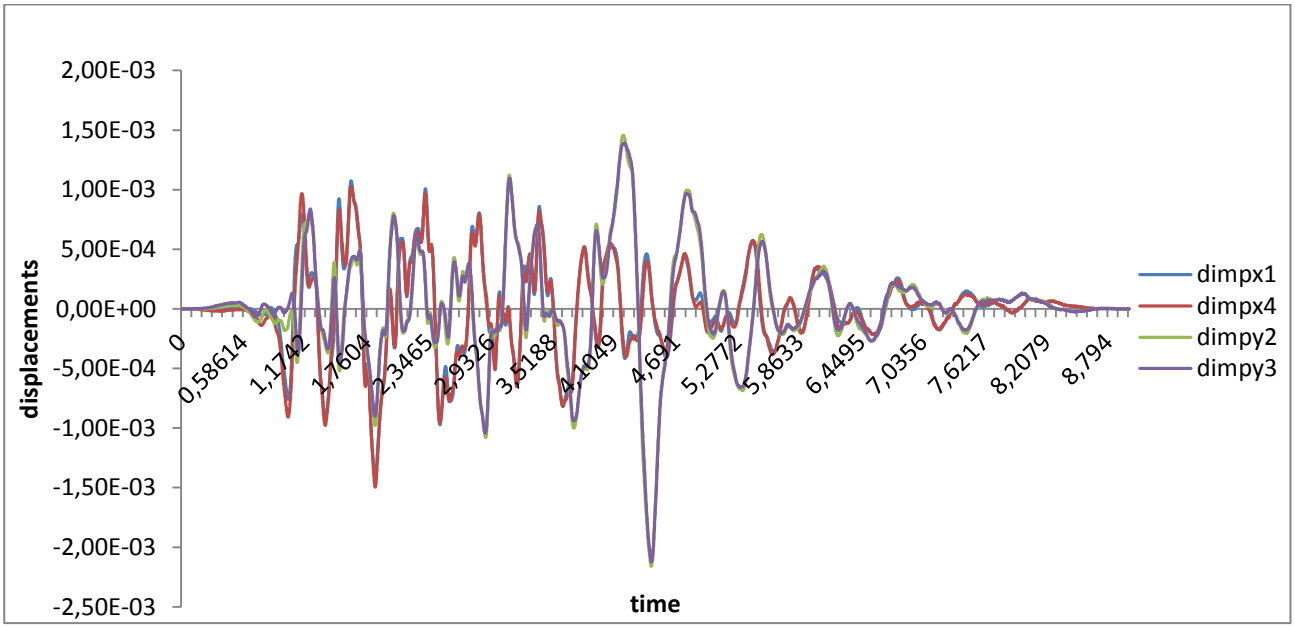

Figure 23: imposed displacements at RUN#9

3.6 DIFFICULTIES AND PROBLEMS

The high complexity of the Cast3m model led to several problems during computation.

A 3D elements model concerns a high number of DOF and adding a nonlinear material law, it makes the computational cost very heavy (in this case 6590 points…).

The FE method requires in fact to calculate the stiffness matrix for every element, including all the internal variables described in the material law, at each displacement increment and, as a result of it, the entire process demands some days to finish.
Storing all the data at each time step occupies a large part of the computer memory so, in order to make the storing easier it was chosen insert an algorithm for saving data just every 10 load increments, which gives enough information about the displacements and damage history.
Like every approximation process, a convergence criterion is needed: for the global problem, it's set as $\left|f^{ext} - f^{int}\right| \leq \varepsilon$ while for the local iterations the criteria are the ones specified above for the internal variables.
The convergence is not reached in two cases: the maximum number of sub steps had been made and the residual is increasing instead of decreasing.
Considering the weakest seismic load applied, there are no convergence problems until the displacements gradient is small but when it starts increasing (e.g. at time 0,9-1,5 in RUN#9), the fem program begins to show some difficulties: the number of damaged elements grows up quickly during the same load step and the convergence criterion diverges. The main trouble is that during this step iteration, all the values become NaN (Not a Number).
The fact that reducing the imposed displacements at 0,1 led to the end of the calculation without any non-convergence issue might had suggest that the problem lied in the material law: it has been found out that there's a non-convexity of the threshold surfaces and it brings some issues during the return mapping integration (Oritz & Simo, 1986), together with the fact that the complex state of charge imposed is not radial. It was then decided to go on with the structural analysis by introducing another concrete's law: Ricrag model. Similar to the previous one, it's still based on the thermodynamic potential but it's not able to take in account the unilateral effect phenomenon (stiffness gain when switching from tension to compression) (Richard B. , Ragueneau, Cremona, & Adelaide, 2010).
In order to overcome the computational problems, it was suggested to go back to the Ricbet model and change the parameters using those (annex 4) computed at CEA (using the same constitutive law but applied to a plate model):

- a smaller crack closure stress to reduce the range where the threshold surfaces are having shape issues;
- a lower precision (10E-3 instead of 10E-8) to facilitate convergence.

The problem of reducing precision may withdraw the exact solution of the dynamic problem so the results are probably going to be less accurate.

4 RESULTS

In the pursuance of validating the models described in the previous chapters, the results have to be analyzed and compared to each other.

The time history analysis is launched for each one of the seismic inputs and the outputs are given in terms of:

- Acceleration, speed and displacement along the three axes x, y and z, for every prescribed point of anyone of the 3 floors;
- Stress field for all the mesh points;
- Internal variables, including damage D, for the entire structure.

Concerning the comparison between the numerical results and the experimental data, the displacements and accelerations at ground floor and at the 3rd floor are investigated.

4.1 RUN#9

Here are reported the RUN#9 data purchased with the Ricbet constitutive model and compared to the experimental data supplied from the benchmark organization committee.

4.1.1 Displacements

First of all, the displacements along x and y at the ground floor are compared: knowing that the shaking table is a very rigid body, a close similitude between the numerical and experimental fields could be expected, for any structure constitutive law.

This forecast is confirmed in the graphs below:

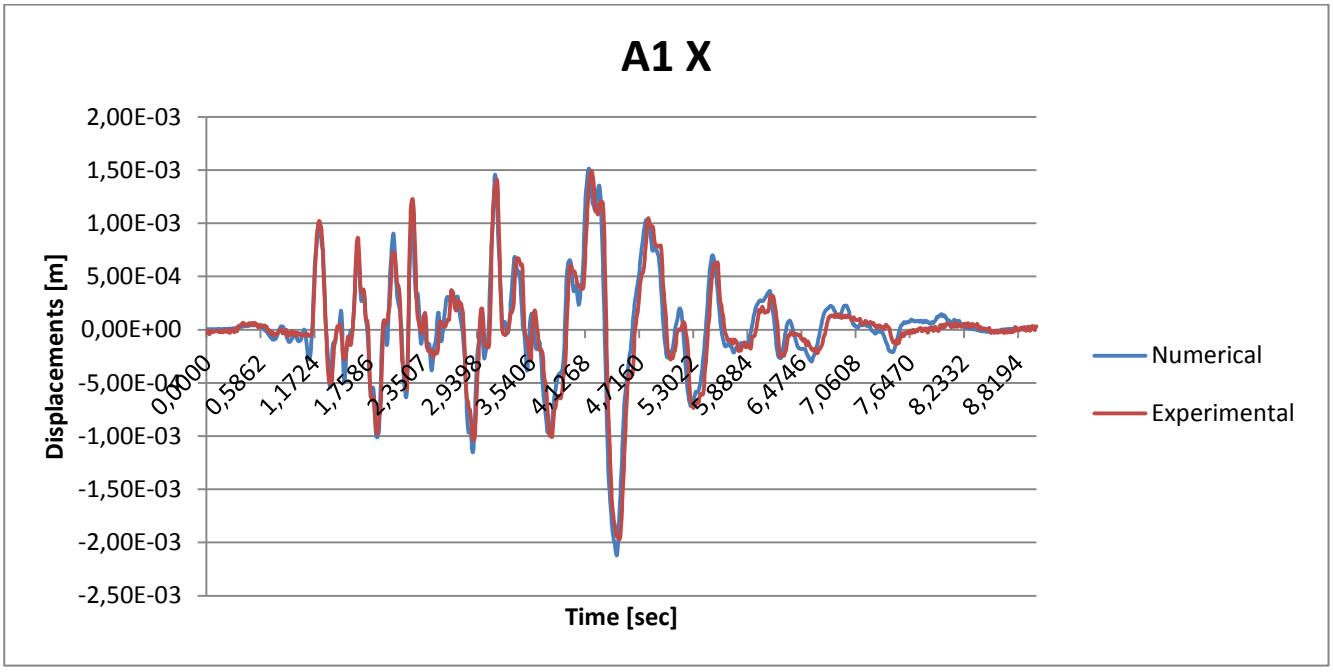

Figure 24 : Numerical and experimental displacements along x for point A, ground floor

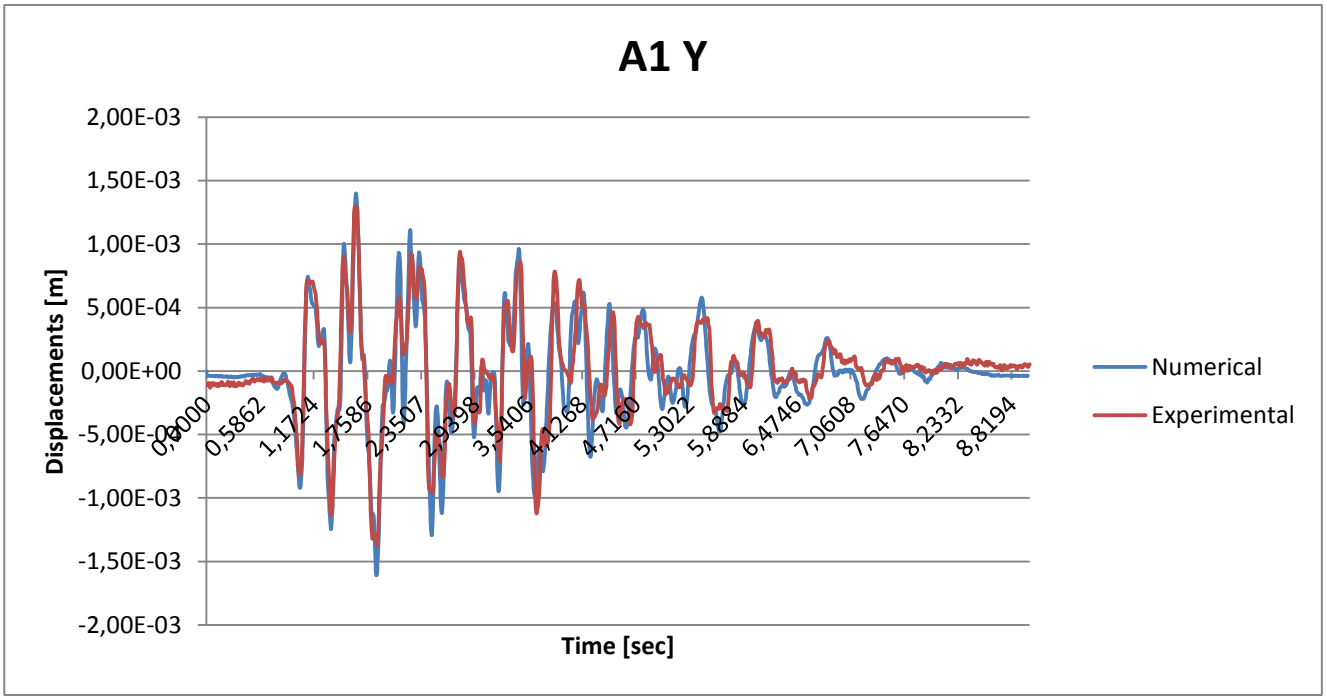

Figure 25: Numerical and experimental displacements along y for point A, ground floor

One can expect that at the highest level (3rd floor), the displacements should became wider because of mainly two factors:

1. The asymmetric shape of the structure and the complexity of the imposed displacements leads to torsional behaviors, which have to be added to the simple x and y displacements;
2. The constitutive law for concrete gives the structure a deformable-body behavior, causing loss of stiffness and incrementing the displacement field.

This event is confirmed in the table below, where the maximum and minimum displacements for each second have been isolated at ground level and at 3rd floor of point D, which is expected to be one of the most subjected to the effects mentioned above.

Table 6: Max and min displacements entity at D1 and D3

second	Min x Numerical [m]		Min x Experimental [m]	
	Ground level	3rd floor	Ground level	3rd floor
0	-1,9615E-04	-6,9036E-04	-5,5233E-05	-1,7244E-04
1	-1,1412E-03	-2,7970E-03	-8,3007E-04	-2,2142E-03
2	-1,3437E-03	-3,7837E-03	-1,1322E-03	-3,0874E-03
3	-9,9695E-04	-2,5199E-03	-8,4115E-04	-2,3548E-03
4	-2,0981E-03	-3,2375E-03	-1,9725E-03	-2,5053E-03
5	-8,8933E-04	-1,6098E-03	-7,3766E-04	-1,2087E-03
6	-4,1762E-04	-1,0186E-03	-2,0421E-04	-2,6197E-04

7	-3,1650E-04	-7,1540E-04	-1,5086E-04	-1,8067E-04
8	-9,4715E-05	-3,6328E-04	-4,6644E-05	-9,5803E-05
9	-1,1412E-03	-2,7970E-03	-5,5233E-05	-1,7244E-04

second	**Max x Numerical [m]**		**Max x Experimental [m]**	
	Ground level	**3rd floor**	**Ground level**	**3rd floor**
0	5,6668E-06	-7,2383E-05	1,3892E-04	2,0757E-04
1	1,3330E-03	2,5094E-03	1,3164E-03	2,9684E-03
2	1,3344E-03	2,7778E-03	1,4907E-03	3,0472E-03
3	1,8134E-03	3,6435E-03	1,8690E-03	4,0040E-03
4	1,7267E-03	3,0067E-03	1,6226E-03	2,9506E-03
5	7,2047E-04	9,0393E-04	7,4542E-04	1,2626E-03
6	3,2098E-04	2,8261E-04	3,5920E-04	7,5566E-04
7	7,8742E-05	-1,2806E-04	1,1490E-04	3,3205E-05
8	2,9895E-05	-1,5352E-04	5,1518E-05	2,9322E-05
9	1,3330E-03	2,5094E-03	1,3892E-04	2,0757E-04

The numerical data are still in a good correspondence with the experimental ones, as shown in fig. 26:

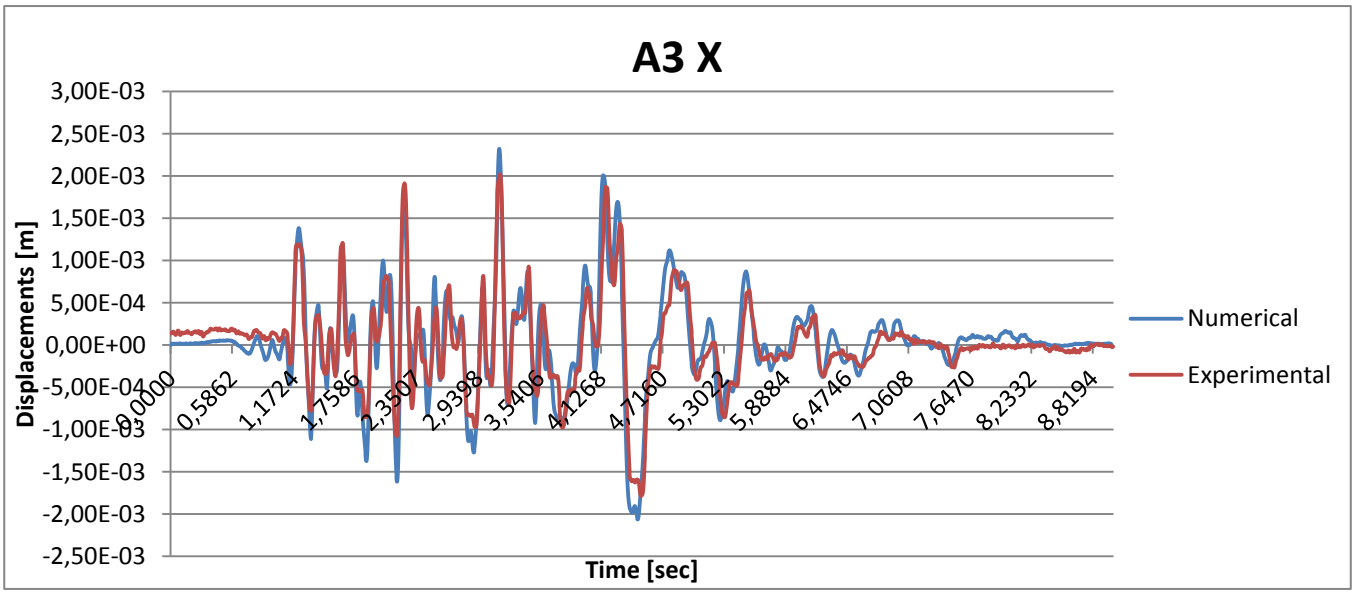

Figure 26: Numerical and experimental displacements along x for point A, 3rd floor

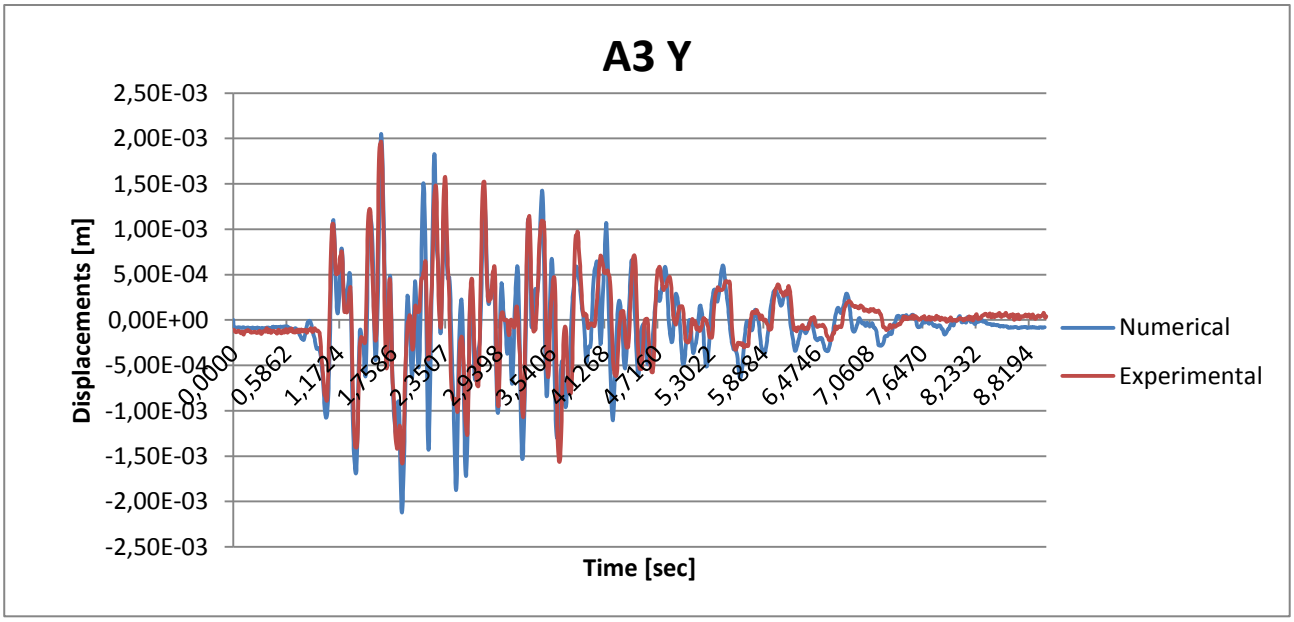

Figure 27: Numerical and experimental displacements along y for point A, 3rd floor

4.1.2 Accelerations

The outputs have been compared also in terms of accelerations and, as it requires two derivations in time since the displacements, two constant are lost and the results are expected to be less accurate.

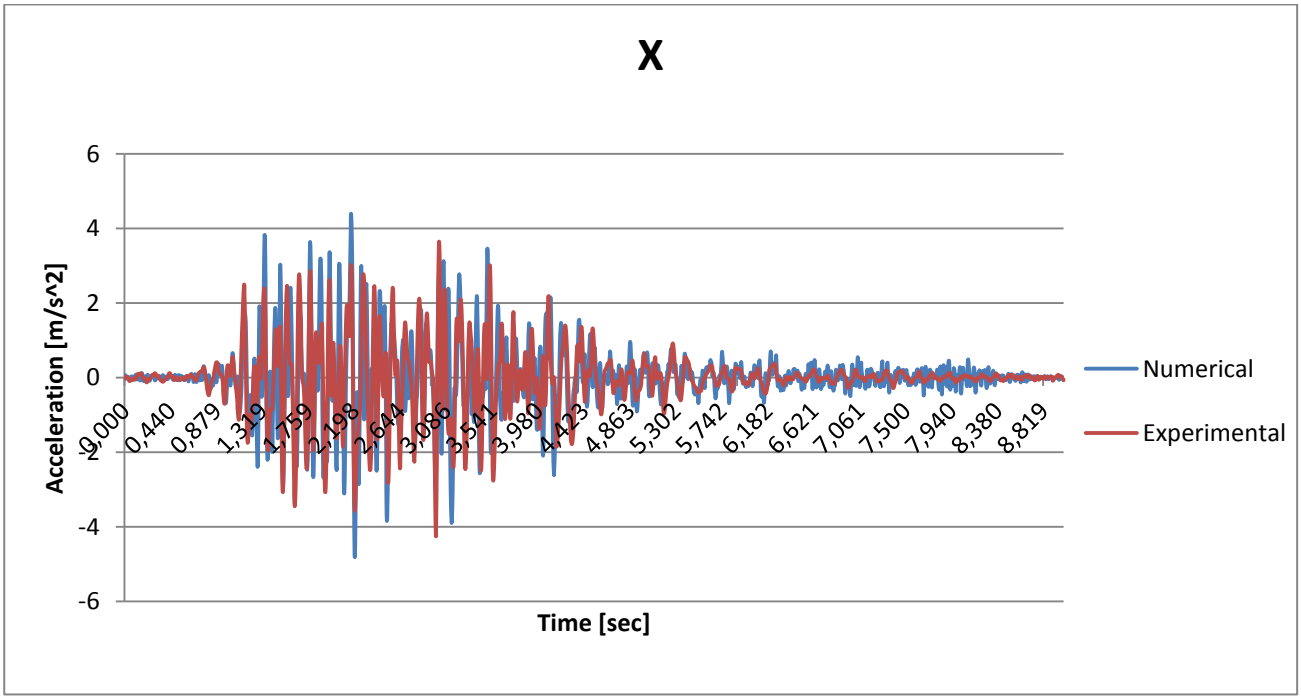

Figure 28: Numerical and experimental accelerations, point A 3rd floor

In order to compare the accelerations, the response spectra have been created as in fig. 29, and it can be stated that the numerical model could be still considered trustworthy.

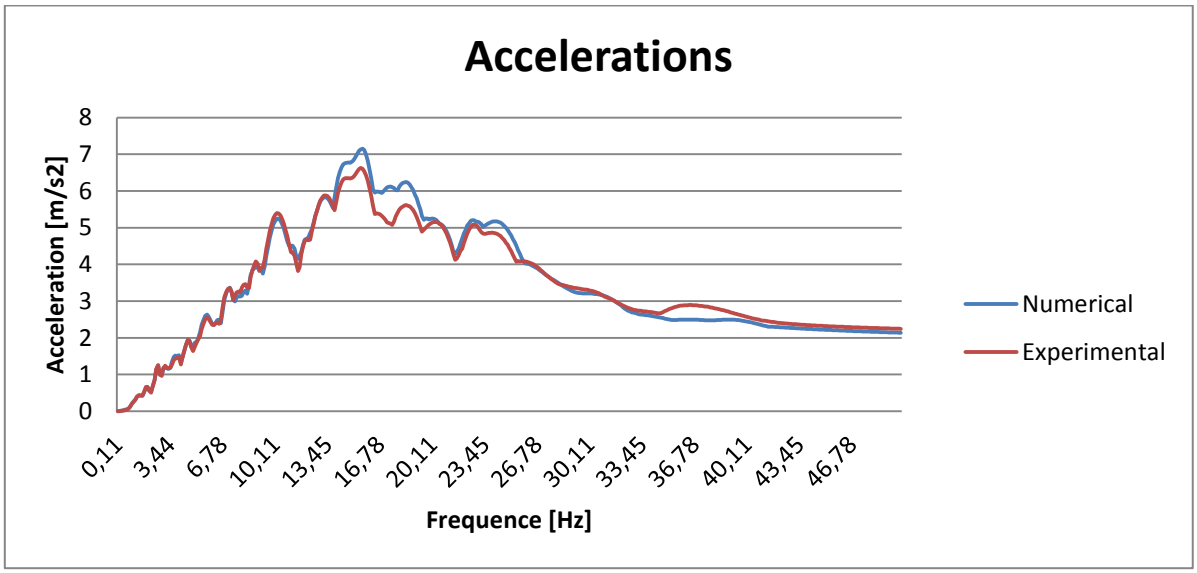

Figure 29: Response spectra

4.1.3 Damage

The complex constitutive law chosen for the concrete nonlinear behavior lets easily identify the most damaged parts of the structure thanks to the damage parameter “D”, as shown in fig. 30.

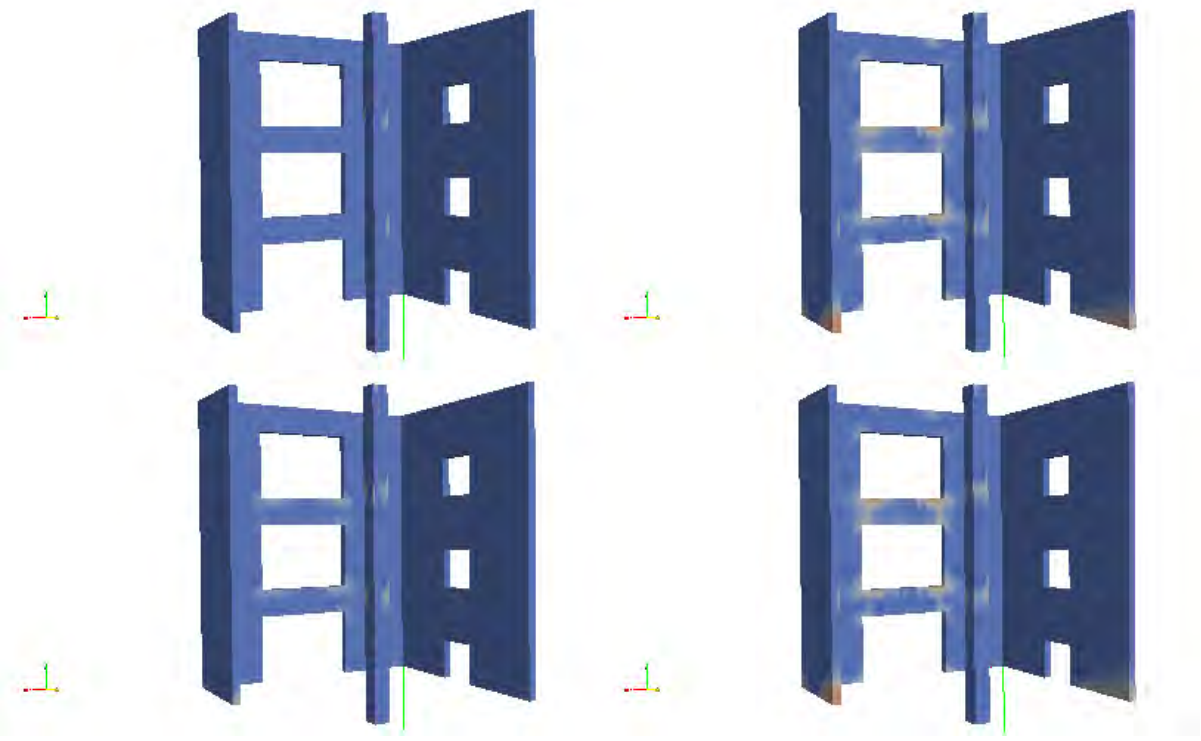

Figure 30: damage at times 0 sec, 1.4 sec, 4 sec and 8 sec

The damaged zones are mainly evolving during the most intense seismic inputs and they seems to be mostly localized:

- around the windows corners: here there is an accumulation of stresses due to the absence of material. More specifically the internal variables of the concrete constitutive law are normally averaged in the surroundings of the nodes but the presence of a hole in the surface (the window in this case) makes the variables being averaged in less space, leading to a concentration of stresses and then damage.
- At the lateral walls bases: these zones are the most solicited by the seismic action. In fact the presence of mass in the higher levels causes a great shear force at the base, augmented by the torsional effects occurring because of the asymmetric shape and loads.
- In the central column: this damage localization could be explained both because of the same shear mechanism acting in the walls, and also because of the presence of a rigid floor diaphragm (not deforming in the horizontal plane).

4.2 RUN#19

This run is characterized by a strong acceleration (1.78g) so that the expected results should show an increment of the monitored values, such as displacements lengths, accelerations and damage level and area.

Once again the numerical results seem to be well fitting the experimental ones when referring to the displacements field even looking at the 3rd floor.

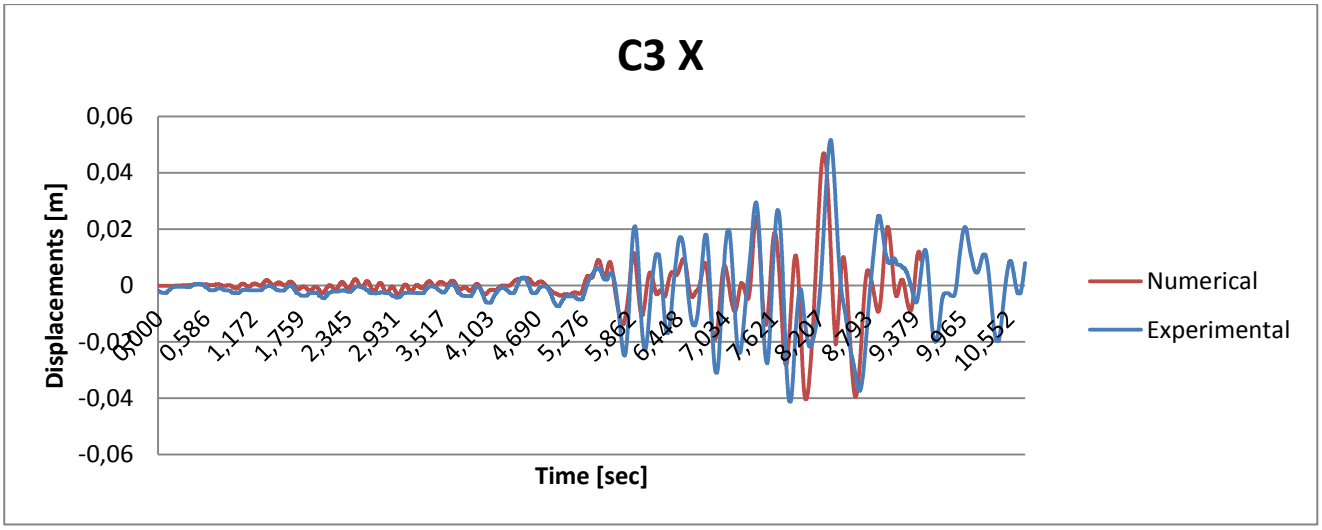

Figure 31: Numerical and experimental displacements along x for point C, 3rd floor

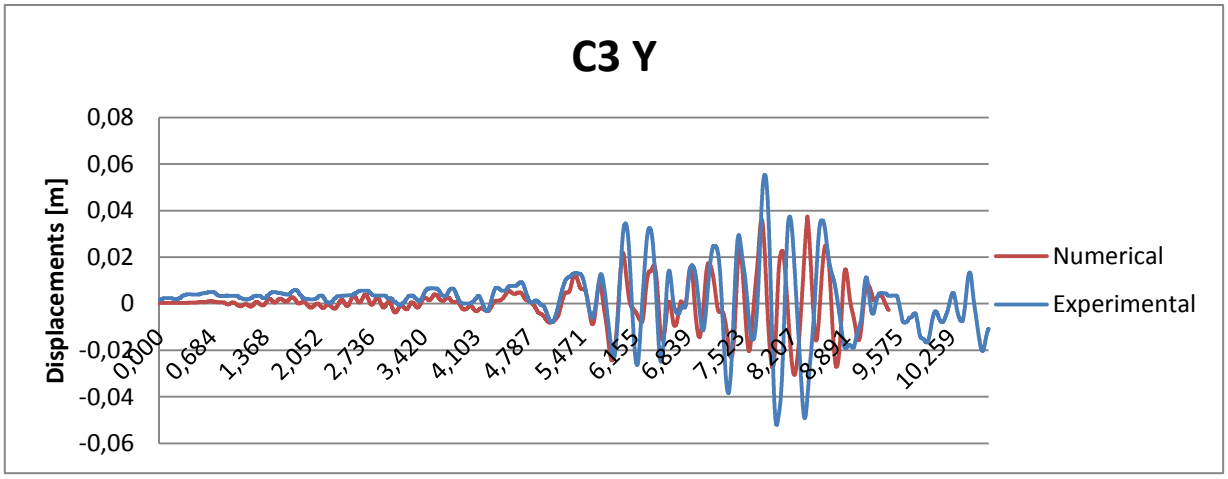

Figure 32: Numerical and experimental displacements along y for point A, ground floor

In this case one can notice that the results are a little less accurate than the previous case, as the differences between the numerical and experimental peak values highlight (tab. 7):

Table 7: Greater values for the difference of peak values than RUN#9

second	Numerical		Experimental			
	min x	min y	min x	min y	diff x	diff y
0	-6,7006E-04	-8,8576E-04	-6,2235E-04	-1,8468E-03	6,1653E-08	-2,6262E-06
1	-1,8446E-04	-1,3822E-03	-3,9132E-04	-3,6652E-04	-1,1910E-07	1,7761E-06
2	-2,1596E-03	-2,0515E-03	-2,4377E-03	-1,3528E-03	-1,2785E-06	2,3788E-06
3	-2,5166E-03	-1,7629E-03	-2,4790E-03	-1,8037E-03	1,8828E-07	-1,4563E-07
4	-2,0124E-03	-3,0349E-03	-2,0701E-03	-6,5445E-04	-2,3540E-07	8,7826E-06
5	-3,3591E-03	-6,8851E-03	-5,2978E-03	-1,9911E-03	-1,6783E-05	4,3440E-05
6	-1,2297E-02	-1,8973E-02	-1,8756E-02	-2,4486E-03	-2,0055E-04	3,5399E-04
7	-1,3158E-02	-8,0813E-03	-2,2641E-02	-1,0311E-03	-3,3945E-04	6,4245E-05
8	-3,2297E-02	-1,8580E-02	0,0000E+00	-2,2811E-03	1,0431E-03	3,4002E-04
9	-3,3012E-02	-1,5066E-02	-3,1328E-02	-1,8468E-03	1,0830E-04	2,2356E-04
10	-6,6475E-03	-7,7582E-03	-3,5857E-03	-1,8468E-03	3,1332E-05	5,6779E-05
second	Numerical		Experimental			
	max x	max y	max x	max y	diff x	diff y
0	5,9271E-04	5,9174E-04	1,8754E-03	8,5105E-04	-3,1656E-06	-3,7413E-07
1	1,6068E-03	1,6261E-03	1,1787E-03	1,1713E-03	1,1926E-06	1,2720E-06
2	8,6875E-04	1,5533E-03	3,2113E-04	1,1713E-03	6,5160E-07	1,0409E-06
3	1,6804E-03	2,2579E-03	1,0849E-03	1,5272E-03	1,6467E-06	2,7660E-06
4	1,5105E-03	2,4863E-03	1,7910E-03	2,1950E-03	-9,2596E-07	1,3634E-06
5	2,8228E-03	4,7615E-03	4,4419E-03	4,9033E-03	-1,1762E-05	-1,3708E-06
6	8,0811E-03	1,0031E-02	1,4032E-02	9,7339E-03	-1,3160E-04	5,8720E-06
7	7,2962E-03	1,5146E-02	1,4537E-02	1,6204E-02	-1,5809E-04	-3,3178E-05

8	1,6715E-02	9,9989E-03	2,0910E-02	1,4693E-02	-1,5785E-04	-1,1591E-04
9	3,8591E-02	1,3321E-02	3,6787E-02	2,3204E-02	1,3598E-04	-3,6099E-04
10	1,5307E-02	1,6535E-02	1,1953E-02	1,4032E-02	9,1448E-05	7,6490E-05

The difference of the squares of the peak values was generally 10 times smaller in RUN#9, but these values are acceptable anyway.

Comparing the global displacements history, as it stands out in fig. 33, one can notice that the points D and C are the most influenced by torsional effects, and that the torsional center lies next to point A: it could be explained thanks to the presence of the two main rc walls crossing in point A, giving a major value for stiffness around this corner.

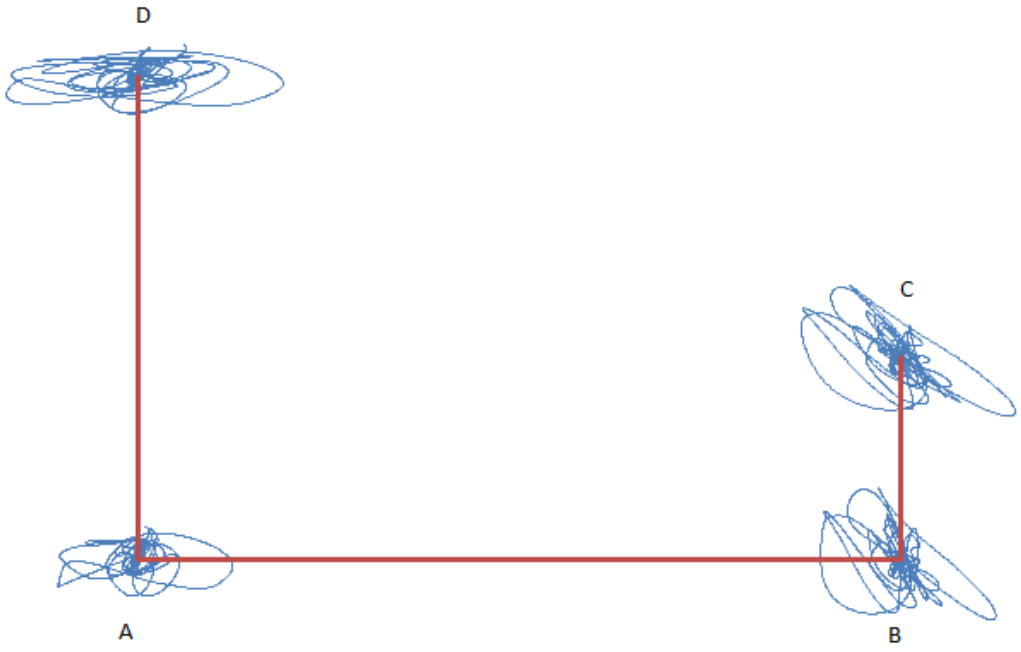

Figure 33: Displacements at each monitored point, 3rd level

4.2.1 Damage

As for the previous run, the damage-based model for concrete behavior let easily identify the zones in which nonlinearities occurred (fig. 34). Once again, the most injured parts are those at the lateral walls bases and around the windows corners, in addition to the central column where the horizontal slabs are anchored.

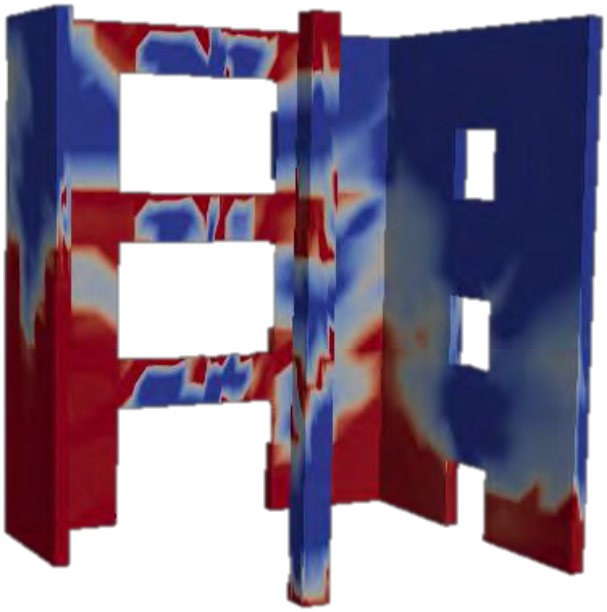

Figure 34: Damaged zone at the end of RUN#19

4.3 RUN#23

The last test is about an “aftershock”: a weaker earthquake occurring a few time after a big one.

During the experimental tests, this seismic signal has been submitted to the structure already damaged by the Northridge earthquake (RUN#19).

Knowing that the numerical model is working properly, this run could be used to mark the differences between a “healthy” structure and a damaged one.

Here are reported the displacements curves:

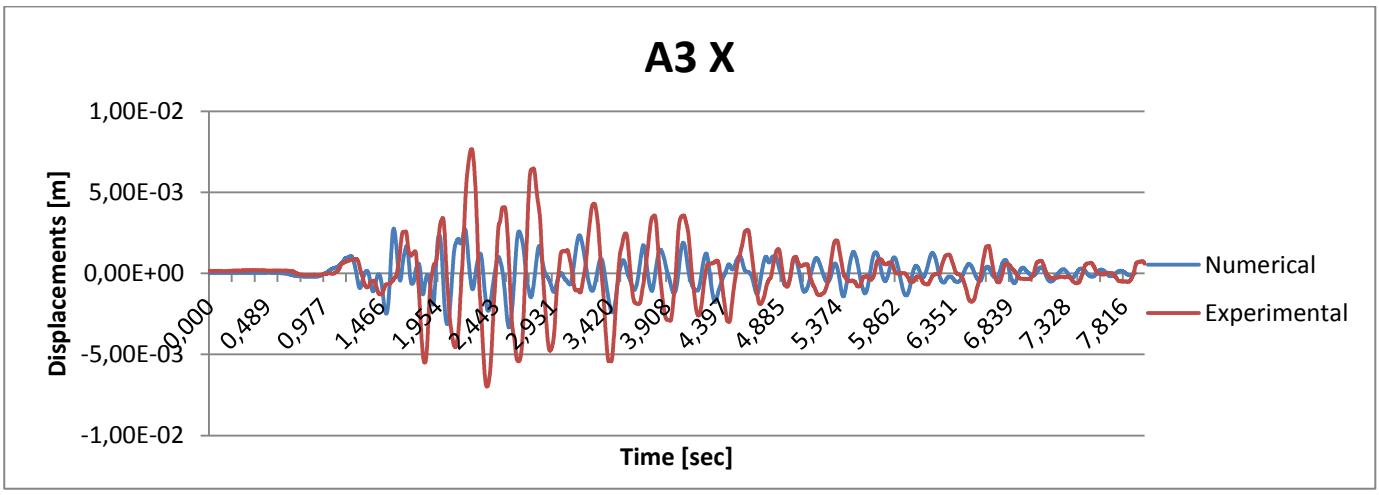

Figure 35: Numerical and experimental displacements along x for point A, 3rd floor

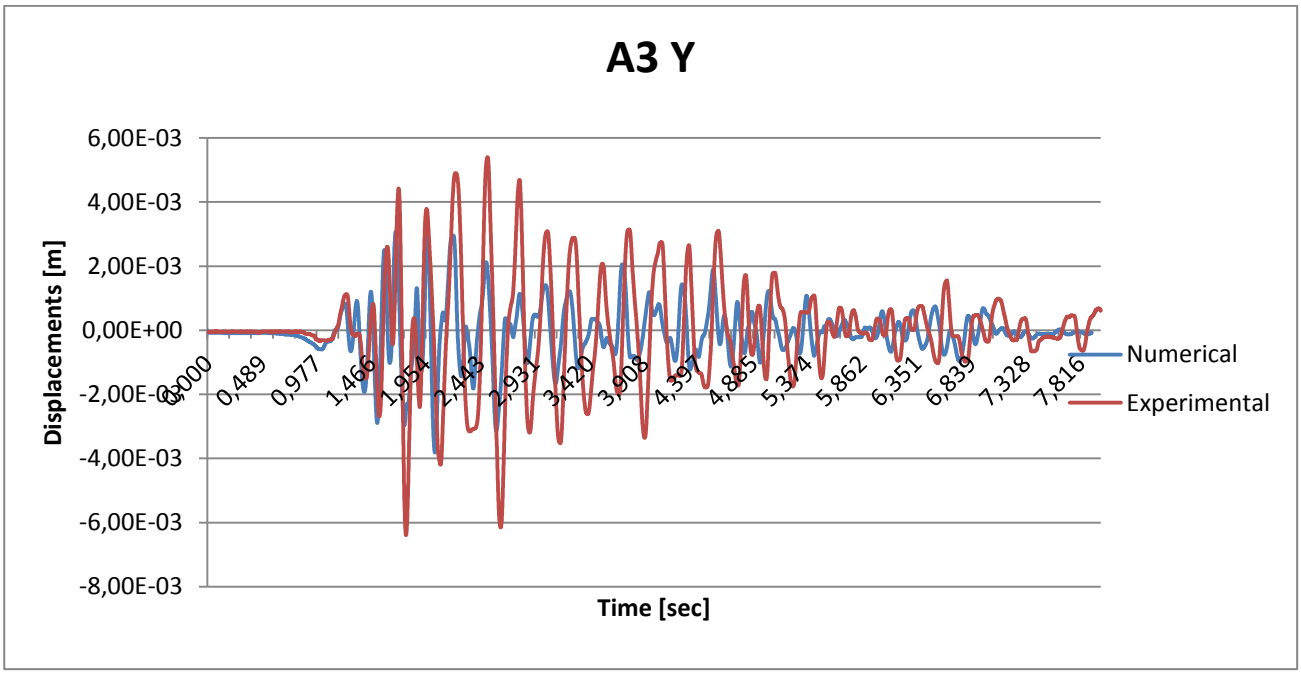

Figure 36: Numerical and experimental displacements along y for point A, 3rd floor

It is clear that the experimental displacements, corresponding to a damaged structure, are much greater than the numerical ones, corresponding to the healthy structure. This fact could be explained by highlighting the fact that during an earthquake the building is going to damage, leading to a loss of stiffness

Moreover the disposition of the experimental peak values "not in phase" with those numerical, is confirming the stiffness loss: the structure period is strictly connected to the stiffness matrix through the expression $\omega = \sqrt{k/m}$.

4.4 Strength Reduction Factor

The seismic analyses have been carried on once again by giving materials a simply linear elastic constitutive law and what stood out is that, for the RUN#9, the results remain the same as for considering nonlinear material (as shown in fig. 37): it means that during a 0.2g earthquake, this structure mainly remained in the elastic field.

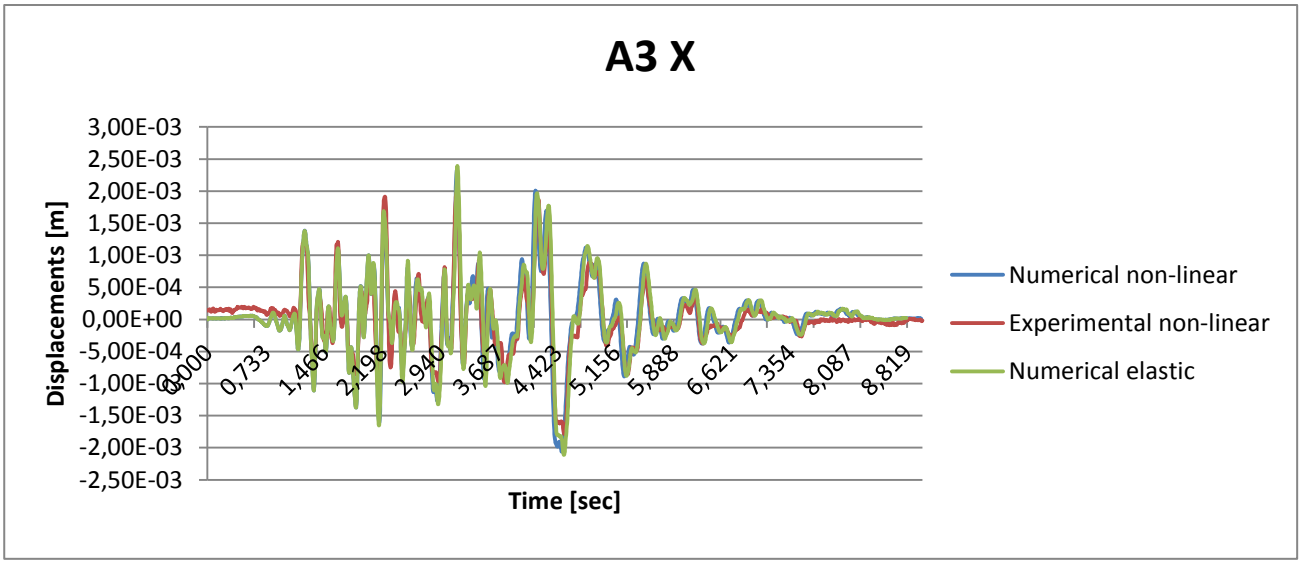

Figure 37: Non-linear and elastic models displacements along x, 3rd floor

Considering the major intense earthquake in RUN#19, the damage evolution affects more seriously the building bases so that a different response between elastic constitutive law and the inelastic one can be easily predicted. As it is highlighted in fig 35, the elastic response in terms of displacements is wider despite the inelastic one: that's because with the elastic constitutive law, the structure has no dissipation mechanisms and no loss of stiffness represented.

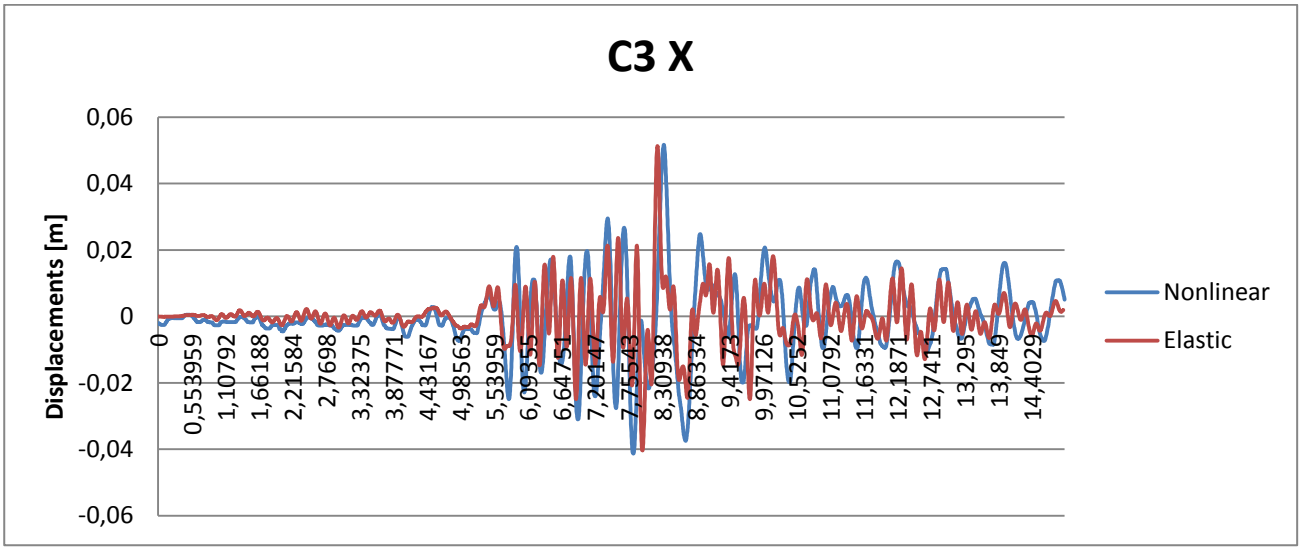

Figure 38: Elastic and inelastic models displacements, point C 3rd floor

In the engineering practice it means that building up a structure resisting to an earthquake without damaging would require bigger dimensions in design and more material quantities and, as a consequence of it, increasing costs.

On the other side it's more common, in everyday practice, to carry on elastic equivalent analysis because they don't demand very high computational costs and, in the pursuance of keeping in account dissipation mechanisms due to nonlinearities, several Strength Reduction Factors have been developed.

One of the first developed principles is that the lateral strength, in seismic design, is much higher than the real lateral strength needed to keep the structure in the elastic domain and it can be reduced by the ratio:

$$R_\mu = \frac{F_y(\mu = 1)}{F_y(\mu = \mu_i)}$$

where above there is the lateral yielding strength for maintaining the system elastic, while under there's the lateral yielding strength to maintain the displacement ductility under a maximum tolerance (Miranda & Bertero, 1994).

Nowadays in the Eurocode 8 are reported specific reduction factors, which have to be applied to the design spectra in order to reduce the seismic forces. In this case of study in particular it has been chosen to calculate the reduction factor as

$$q = \frac{d_e}{d_s}$$

where d_s is the average value for the interstorey drift for the nonlinear model, and d_e is the interstorey drift for the elastic model.

Table 8: Strength reduction factor for displacements D3

	d_{el}/d_s			
	Min x	**Min y**	**Max x**	**Max y**
	9,9744E-01	1,0028E+00	9,3018E-01	9,9835E-01
	1,0016E+00	9,8843E-01	1,0018E+00	1,0014E+00
	9,9720E-01	9,9999E-01	9,9865E-01	1,0011E+00
	1,0004E+00	9,9875E-01	9,9787E-01	1,0004E+00
	1,0599E+00	1,0007E+00	1,0036E+00	1,0003E+00
	1,0016E+00	9,8774E-01	1,0018E+00	1,0014E+00
	1,0185E+00	9,2862E-01	1,1660E+00	1,1660E+00
	1,3200E+00	1,7339E+00	1,1177E+00	1,1177E+00
	1,2921E+00	9,1190E-01	1,3689E+00	1,3689E+00
	9,1867E-01	1,1040E+00	9,2552E-01	9,2552E-01
	1,7519E+00	8,3047E-01	6,9517E-01	6,9517E-01
Average	**1,1236E+00**	**1,0183E+00**	**1,0402E+00**	**1,0251E+00**

The reduction factor q found in this case corresponds to 1,12 after choosing to consider the major value from those calculated.

5 CONCLUSIONS

The benchmark project SMART 2013 was launched with the aim of raising the knowledge on torsional and nonlinear behavior of RC structures in order to predict their vulnerability when a seismic event occurs. In order to that, the campaign organizers are charged of comparing and validating the various approaches used for the dynamic responses.

The LMT Cachan is taking part to the project and built his own numerical model: 3D cubic elements are chosen for a more detailed representation of the perimetral walls and the central column, while elastic plates are modeling the floor diaphragms and beam element well-fitting the reinforcement steel bars. After explaining the importance of taking in account the shaking table, its plate elements model provided by CEA is assembled to the superstructure one. Once the assumptions made for the numerical model have been validated by a modal analysis and an elastic calibration, the nonlinear constitutive laws for steel bars and concrete are presented: a simple uniaxial model (Menegotto-Pinto) adapted to represent a cyclic behavior for the steel, and the Ricbet model for the concrete. This last one had been implemented to recreate softening and damage in tension, internal sliding and kinematic hardening with stiffness recover (unilateral effect) thanks to a cracks closure variable, and plasticity with isotropic hardening in compression. A regularization technique based on fracture energy is then explained to avoid mesh dependency.

The time-history dynamic analysis principles are later on reported and set up with the prescribed seismic inputs: the numerical computation generated some problems due to the high computational cost required and some non-convergences caused by non-radial loadings.

After having examined numerical and experimental results in terms of displacements, a good correspondence between the two data sets can be stated, both for the weaker and the strongest earthquakes. As expected, at the base level there are no remarkable differences between numerical and experimental displacements values, growing up when looking at the 3rd floor: the numerical displacements seem to be a slightly wider than the experimental ones but still satisfying.

Damage is mainly localized at the structure bases, as an effect of shear and torsion induced by the seismic solicitations and his values are increasing as the strength of the earthquake increases.

In conclusion I can say that the numerical model computed, coupling 3D elements and Ricbet continuum-damage-based constitutive law is capable of a very good representation

of a reinforced concrete building behavior under seismic loads, even when torsional and local phenomena occur.

This procedure could then be used as a seismic behavior predictor for new and existing building when the knowledge of the possible zones of failure want to be arisen, especially when considering strategic structures such as nuclear centrals.

This analysis model is useful also for further studies about the difference between the seismic response of an intact building and an already damaged one.

More research may be conducted in the pursuance of optimizing the computational cost, which is actually very high, and making this model useful for ordinary seismic analyses.

BIBLIOGRAPHY

Charras, & Di Paola. (2011). *La procédure PASAPAS.* CEA.

Chaudat, T., & Richard, B. (2013). *Presentation of the SMART 2013 International Benchmark.* CEA.

Combescure. (2001). *Modelisation des structures de genie civil sous chargement sismique à l'aide de CASTEM 2000.* CEA.

Di Paola. (2001). *Liste des modèles en mécanique non linéaire.* CEA.

Giry, C., Dufour, F., & Mazars, J. (2011). Stress-based nonlocal damage model. *International journal of solids and structures*.

Grégory, L. (2011). *analyse de l'endommagement des structures de génie civil: techniques de sous-structuration hybride couplées à un modèle d'endommagement anisotrope.*

Hillerborg, Modéer, & Peterson. (s.d.). Analysis of crack formation and crack growth in concrete by means of fracture mechanics and finite elements. In *Cement and concrete research vol.6* (p. 773-782). Pergamon Press, Inc.

Lemaitre, J., Chaboche, J.-L., Benallal, A., & Desmorat, R. (2009). *Mécanique des matériaux solides.*

Lermitte. (2008). *preliminary synthetic results report-Blind predictive benchmark SMART2008.* CEA.

Menegotto, M., & Pinto, P. (1973). method of analysis for cyclically loaded reinforced concrete plane frames including changes in geometry and non-elastic behavior of elements under combined normal force and bending.

Miranda, E., & Bertero, V. (1994). Earthquake spectra.

Oritz, M., & Simo, J. (1986). An analysis of a new class if integration algorithms for elastoplastic constitutive relations. *International journal for numerical methods in engineering*, 353-366.

Pijiaudier-Cabot, G., & Bazant, Z. (1987). Nonlocal damage theory. *Journal of Engineering Mechanics*.

Richard, B., & Ragueneau, F. (2012). Continuum damage mechanics based model for quasi brittle materials subjected to cyclic loadings: formulation, numerical implementation and applications. *Engineering fracture mechanics*.

Richard, B., Ragueneau, F., Cremona, C., & Adelaide, L. (2010). Isotropic continuum damage mechanics for concrete under cyclic loading: stiffness recovery, inelastic strains and frictional sliding. *Engineering fracture mechanics*, 1203-1223.

USGS. (s.d.). *Earthquake Hazard Program*. Tratto da www.usgs.gov: http:/earthquake.usgs.gov

Zareiana , F., & Medina, R. (2009). *A practical method for proper modeling of structural damping in inelastic plane structural systems.*

Zareiana, F., & Medina, R. (2009). A pratical method for proper modeling of structural damping in inelastic plane structural systems.

Zienkiewicz, O., & Taylor, R. (s.d.). *The finite element method.*

ANNEXES

ANNEX 1: MOCK-UP GEOMETRY

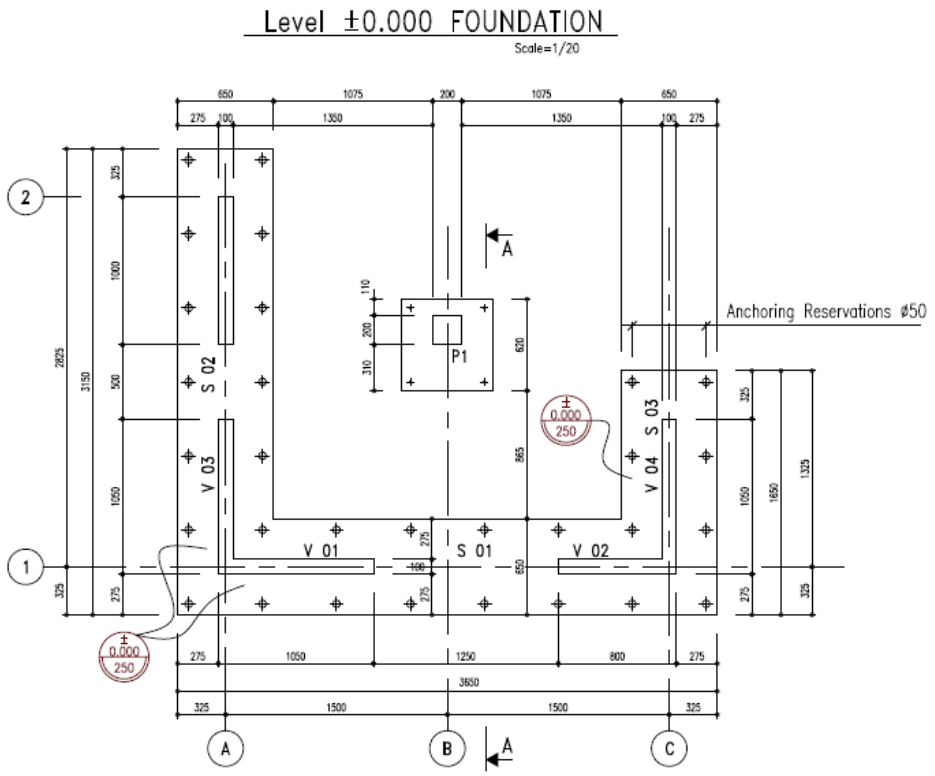

Figure 39: Mock-up foundations

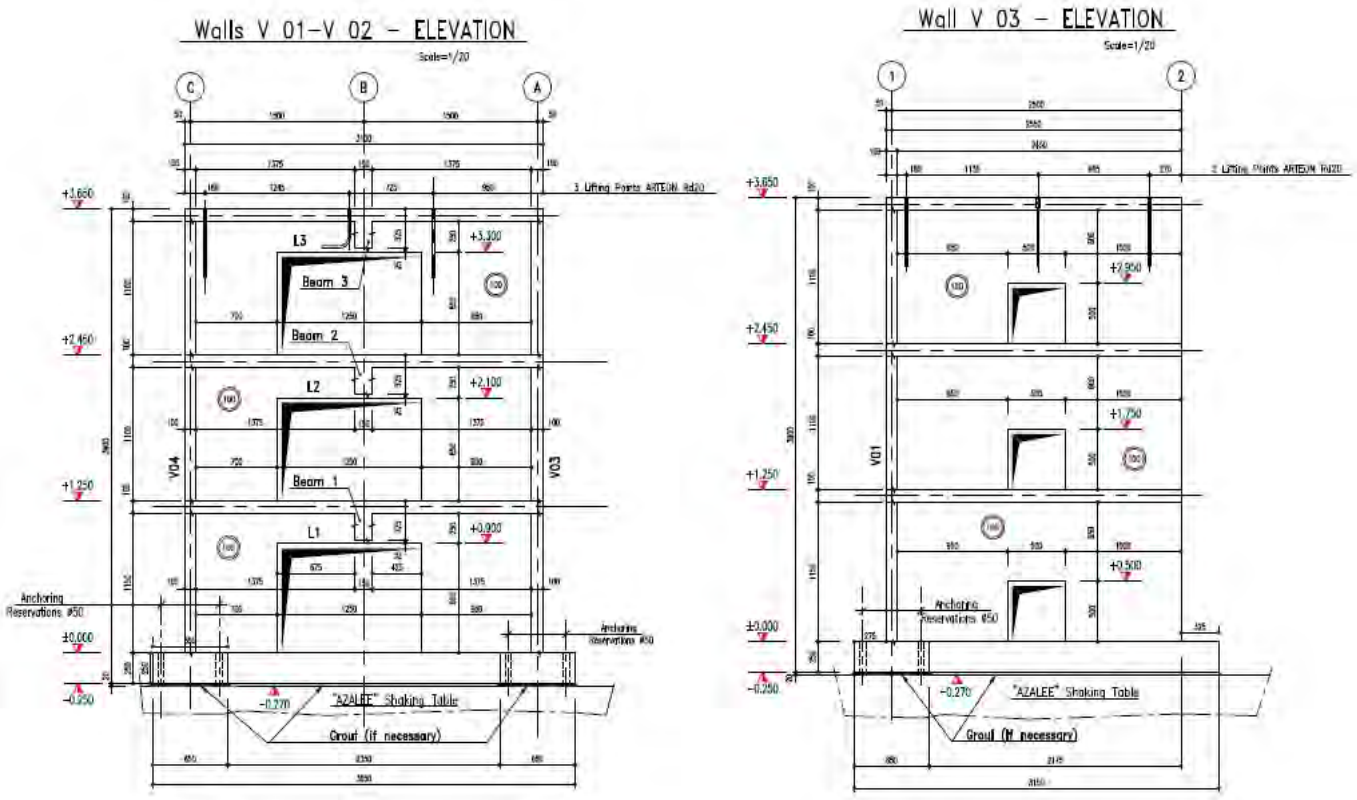

Figure 40: Elevation walls with windows

ANNEX 2: CONCRETE PARAMETERS VALUES

Structural component	Property	Young modulus (MPa)	Poisson Ratio	Compressive strength (MPa)	Tensile strength - splitting tests (MPa)	Tensile strength - bending tests (MPa)	Fracture energy ($J.m^{-2}$)	Mass density ($kg.m^{-3}$)
Foundation	Design value	32000	0,20	30,00	2,40	2,40	160,00	2300
	Mean measured value	25400	0,17	43,30	3,45	4,14	135,50	-
	Standard deviation	-	-	1,51	0,30	0,10	20,50	-
Floor #1	Design value	32000	0,20	30,00	2,40	2,40	160,00	2300
	Mean measured value	28200	0,18	41,10	3,25	3,74	136,00	-
	Standard deviation	-	-	0,92	0,40	0,30	6,53	-
Shear walls – cast #1	Design value	32000	0,20	30,00	2,40	2,40	160,00	2300
	Mean measured value	28700	0,19	41,70	3,15	3,89	133,60	-
	Standard deviation	-	-	0,07	0,15	0,24	26,16	-
Floor #2	Design value	32000	0,20	30,00	2,40	2,40	160,00	2300
	Mean measured value	24700	0,17	36,80	3,35	3,32	114,00	-
	Standard deviation	-	-	2,61	0,17	0,17	19,94	-
Shear walls – cast #2	Design value	32000	0,20	30,00	2,40	2,40	160,00	2300
	Mean measured value	25700	0,19	35,50	2,70	3,78	132,00	-
	Standard deviation	-	-	0,85	0,26	0,37	13,45	-
Floor #3	Design value	32000	0,20	30,00	2,40	2,40	160,00	2300
	Mean measured value	24400	0,18	37,80	3,40	3,80	135,00	-
	Standard deviation	-	-	1,45	0,05	0,17	5,40	-
Shear walls – cast #3	Design value	32000	0,20	30,00	2,40	2,40	160,00	2300
	Mean measured value	29500	0,18	46,60	4,00	3,57	123,00	-
	Standard deviation	-	-	4,24	0,30	0,04	12,05	-

Figure 41: Concrete parameters prescribed by CEA

ANNEX 3: PASAPAS ALGORITHM

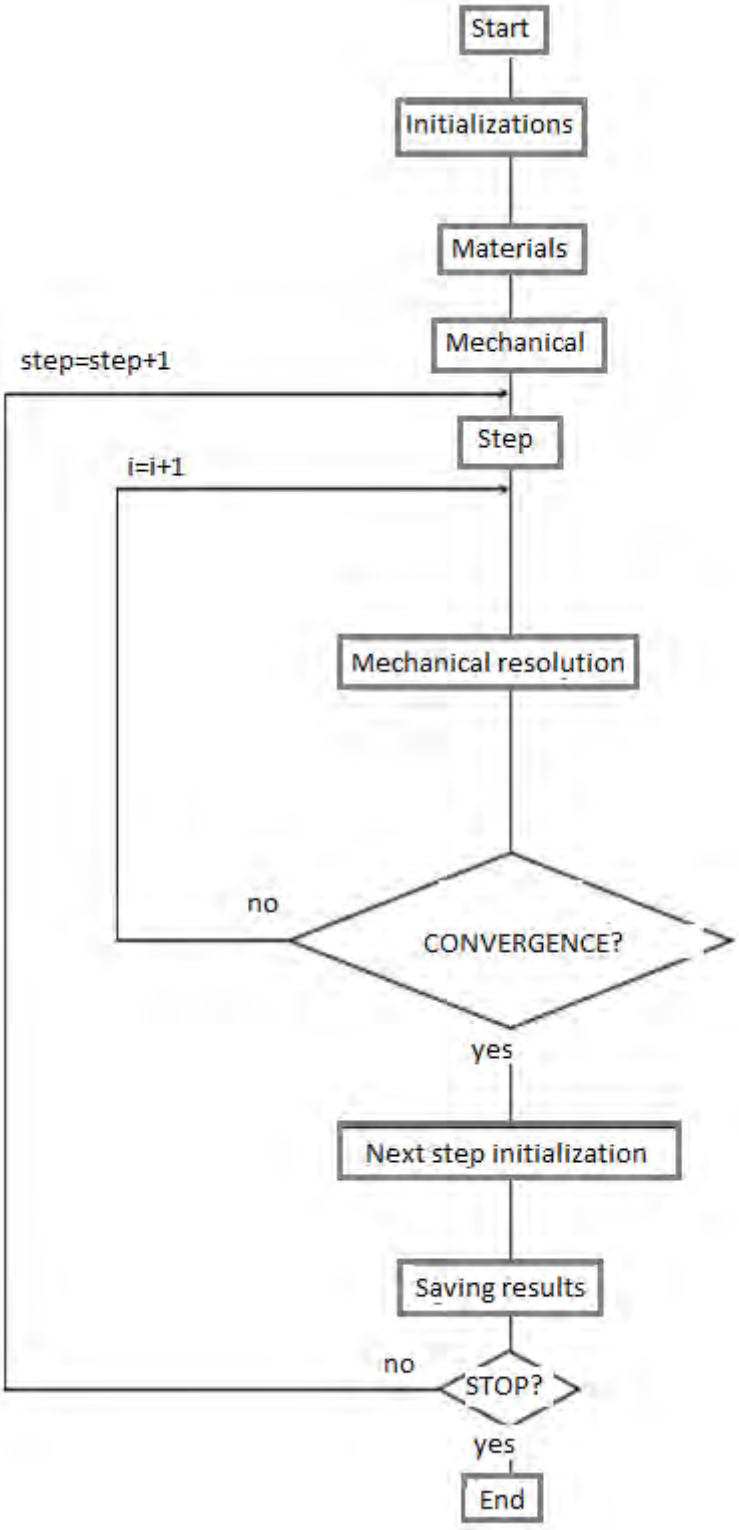

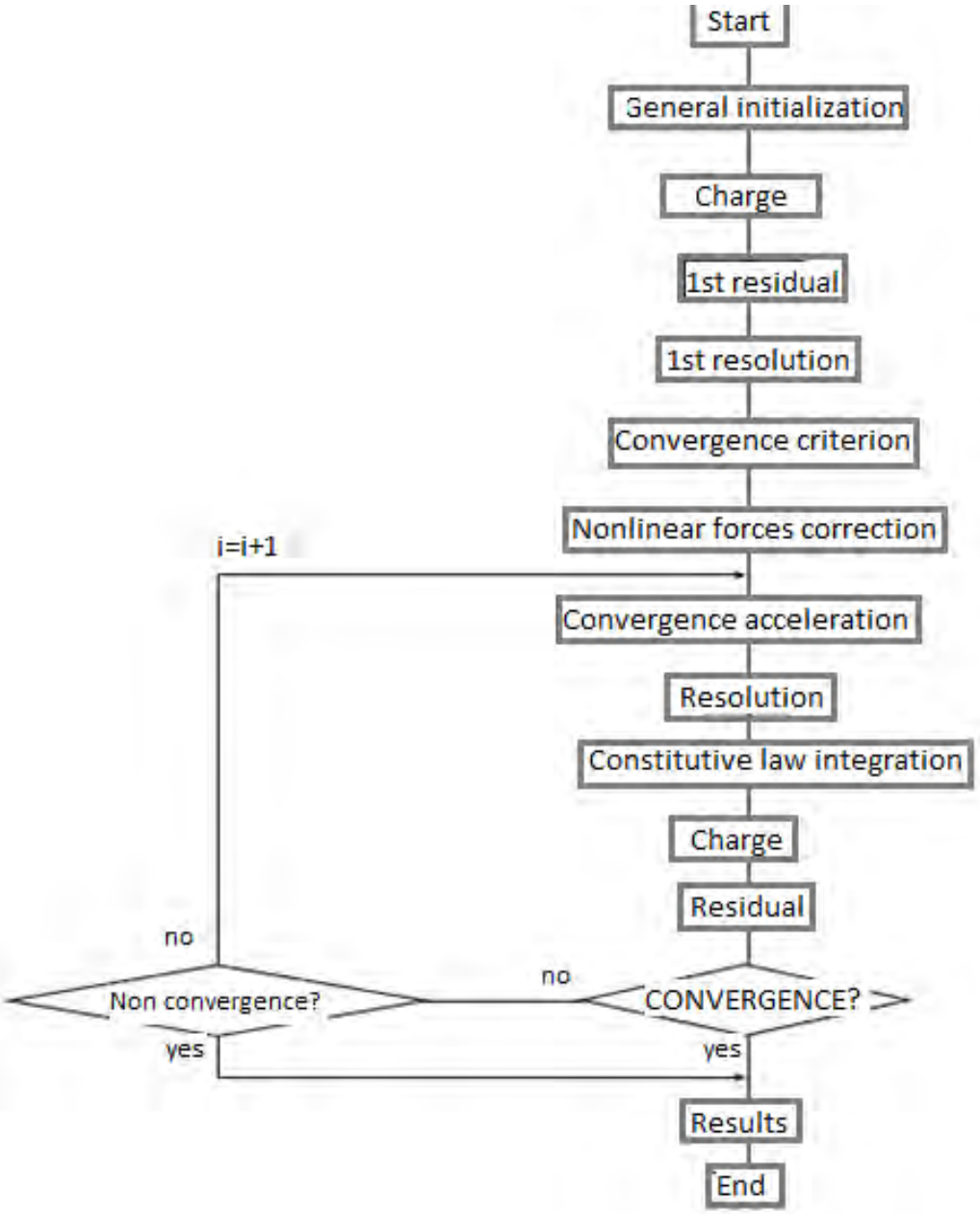

Figure 42: PASAPAS and UNPAS algorithms

ANNEX 4: CEA PARAMETERS VALUES

Table 9: CEA concrete parameters for Ricbet

Properties	Variables	Values
Density ρ [kg/cm^3]	RHO	2300
Poisson's coeff. N	NU	0.2
Hardening modulus 1	GAM1	7.2E7
Hardening modulus 2	A1	8.0E-6
Closure stress [MPa]	SREF	-3.2E7
Brittleness in tension	ALDI	5.92E-3
Yield surface 1	AF	0.72
Yield surface 2	BF	0.27
Plastic potential 1	AG	0.63
Plastic potential 2	BG	0.45
Yield hardening 1	AC	3.1E10
Yield hardening 2	BC	700.0
Asymptotic stress in compression [MPa]	SIGU	-4.0E6
Initial compression strength [MPa]	FC	6.0E7

ANNEX 5: ACCELEROGRAMS

Table 10: seismic inputs

Run	PGA (g)	Type
9	0.20	Real – Design signal - nominal
11	0.20	Scaled – Northridge earthquake – step 1
13	0.40	Scaled – Northridge earthquake – step 2
17	0.80	Scaled – Northridge earthquake – step 3
19	1.78	Real – Northridge earthquake – nominal
21	0.12	Scaled – Northridge after shock – step 1
23	0.37	Real – Northridge after shock – nominal

List of figures

List of tables